



# In-silico identification of small molecule benzofuran-1,2,3-triazole hybrids as potential inhibitors targeting EGFR in lung cancer via ligand-based pharmacophore modeling and molecular docking studies

Sunil Kumar<sup>1</sup> · Iqra Ali<sup>2</sup> · Faheem Abbas<sup>3</sup> · Nimra Khan<sup>4</sup> · Manoj K. Gupta<sup>5</sup> · Manoj Garg<sup>6</sup> · Saroj Kumar<sup>7</sup> · Deepak Kumar<sup>1</sup>

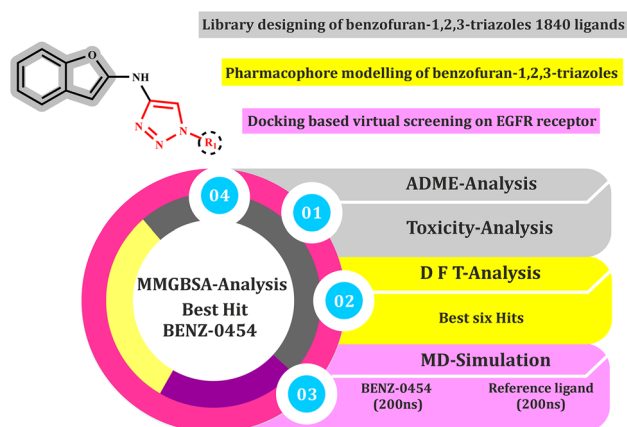
Received: 25 March 2023 / Accepted: 26 July 2023

© The Author(s), under exclusive licence to Springer-Verlag GmbH Germany, part of Springer Nature 2023

## Abstract

Lung cancer is one of the most common and deadly types of cancer worldwide, and the epidermal growth factor receptor (EGFR) has emerged as a promising therapeutic target for the treatment of this disease. In this study, we designed a library of 1840 benzofuran-1,2,3-triazole hybrids and conducted pharmacophore-based screening to identify potential EGFR inhibitors. The 20 identified compounds were further evaluated using molecular docking and molecular dynamics simulations to understand their binding interactions with the EGFR receptor. In-silico ADME and toxicity studies were also performed to assess their drug-likeness and safety profiles. The results of this study showed the benzofuran-1,2,3-triazole hybrids BENZ-0454, BENZ-0143, BENZ-1292, BENZ-0335, BENZ-0332, and BENZ-1070 dock score of  $-10.2$ ,  $-10$ ,  $-9.9$ ,  $-9.8$ ,  $-9.7$ ,  $-9.6$ , while reference molecule  $-7.9$  kcal/mol for EGFR (PDB ID: 4HJO) respectively. The molecular docking and molecular dynamics simulations revealed that the identified compounds formed stable interactions with the active site of the receptor, indicating their potential as inhibitors. The in-silico ADME and toxicity studies suggested that the compounds had good pharmacokinetic and safety profiles, further supporting their potential as therapeutic agents. Finally, performed DFT studies on the best-selected ligands to gain further insights into their electronic properties. The findings of this study provide important insights into the potential of benzofuran-1,2,3-triazole hybrids as promising EGFR inhibitors for the treatment of lung cancer. Overall, this study provides a valuable starting point for the development of novel EGFR inhibitors with improved efficacy and safety profiles.

## Graphical Abstract



**Keywords** EGFR-TKD · Lung cancer · Benzofuran-1,2,3-triazole hybrids · Pharmacophore modeling · ADME

Extended author information available on the last page of the article

## Introduction

According to the World Health Organization (WHO), lung cancer is the most common cancer globally, with an estimated 2.2 million new cases in 2023 (Sharma et al. 2022). It is also the leading cause of cancer deaths, accounting for about 18% of all cancer deaths, or 1.76 million deaths (Thandra et al. 2021). The majority of lung cancer cases are caused by tobacco smoking, but exposure to other risk factors such as air pollution, radon, and occupational exposure to carcinogens can also increase the risk of developing lung cancer (Hofman et al. 2022). Lung cancer is more common in men than women, and the incidence rates vary widely across different regions of the world (Vaccarella et al. 2022). The highest incidence rates are found in North America, Europe, and Australia, while the lowest rates are found in Africa and Asia (Sharma 2022). WHO emphasizes that lung cancer can be prevented by reducing exposure to risk factors, such as tobacco smoking, and by increasing access to early detection and diagnosis, as well as to effective treatment (Kerpel-Fronius et al. 2022). It also highlights that lung cancer is a complex disease and there are multiple subtypes of lung cancer, with different genetic profiles and mutations, therefore the effectiveness of a drug may vary from one subtype to another (Rodriguez-Canales et al. 2016). Overactivation of the epidermal growth factor receptor (EGFR) is a common genetic mutation in lung cancer, particularly in non-small cell lung cancer (NSCLC) (Sahoo et al. 2011). EGFR is a protein that is found on the surface of cells, and it plays a critical role in cell growth and division (Yarden 2001). When mutations occur in the EGFR gene, they can lead to the overproduction of the EGFR protein, which can cause cells to divide and grow uncontrollably, leading to the development of cancer (Sigismund et al. 2018). EGFR mutations are found in about 10–15% of cases of NSCLC (Kumar et al. 2023), and are more common in non-smokers and in patients of Asian descent (Boch et al. 2013). These mutations are typically found in exons 18–21 of the EGFR gene, and they can lead to the overactivation of the receptor (van Assche et al. 2014). Overactivation of the EGFR receptor can be targeted by specific therapies called EGFR tyrosine kinase inhibitors (EGFR-TKIs), which block the activity of the receptor and slow or stop the growth of cancer cells (Zhong et al. 2022). Examples of these drugs are gefitinib, erlotinib, afatinib, and osimertinib. These drugs have been approved by the FDA for the treatment of advanced NSCLC with specific EGFR mutations (Kumar et al. 2021), and they have been shown to improve outcomes in patients with these mutations (Cheng et al. 2022).

Benzofuran-1,2,3-triazole hybrids have been investigated as potential agents for the treatment of lung cancer, as they have been found to have anticancer properties

(Gariganti et al. 2023). For example, some studies have shown that certain benzofuran-1,2,3-triazoles have the ability to inhibit the growth of lung cancer cells and induce apoptosis in lung cancer cells (Liang et al. 2021). One study showed that a specific benzofuran-1,2,3-triazole hybrid compound was able to inhibit the growth of non-small cell lung cancer cells, and another study found that the same compound had an inhibitory effect on lung cancer stem cells (Othman et al. 2022). Several studies have shown that these compounds have activity against various protein kinases, which play an important role in cell proliferation and survival (Sharma et al. 2022), indicating that these compounds may have potential as targeted therapy for lung cancer (Ihn et al. 2015). Benzofurans have been investigated as potential anticancer agents (Napiórkowska et al. 2019), but it's important to note that, there are currently no benzofuran compounds in clinical trials for cancer treatment (Qi et al. 2020).

In this study, we designed benzofuran-based 1,2,3-triazole hybrids and pharmacophore modeling, molecular docking, molecular dynamics (MD) simulation, In-silico ADME, and toxicity studies are performed to understand and to interpret the binding interactions mechanism between the benzofuran-1,2,3-triazole hybrids and the crystallographic EGFR receptor. Overall, this study revealed the presence of potential EGFR inhibitors that possess favorable pharmacokinetic properties. It is anticipated that these results will contribute to the development of more potent and effective drugs to address the issue of lung cancer in humans.

## Materials and methods

### Library designing of benzofuran-1,2,3-triazole compounds

Benzofuran-1,2,3-triazole hybrids are a class of compounds that contain both a benzofuran and a 1,2,3-triazole moiety in the same molecule. These compounds have a wide range of potential applications, including their use as drugs and as materials in electronics and optoelectronics. They may also be used in organic synthesis as building blocks for the construction of more complex molecules. However, more research is needed to fully understand their properties and potential uses. Benzofurans are a class of compounds that have been investigated for their potential as anticancer agents. Some studies have shown that certain benzofurans can inhibit the growth of cancer cells, while others have suggested that they may have the ability to induce apoptosis (programmed cell death) in cancer cells. In this study, we developed a library of 1840 benzofuran-1,2,3-triazole hybrids by introducing various aliphatic and aromatic substitutions at the 10th position of the benzofuran-1,2,3-triazole

hybrids using ChemDraw software. The substituents were chosen based on their suitability for chemical reactions and can be found in (Supporting Table S1) of the supporting data. The designed hybrids were found to have exceptional synthetic accessibility scores and were successfully synthesized. Our primary objective was to create novel and effective anticancer agents that target EGFR in lung cancer. To assess the potential of the designed hybrids as anticancer agents, they underwent testing and evaluation by using in-silico experiments. The findings of this study have the potential to contribute to the development of more potent and drug-like molecules to combat human lung cancer. The strategy presented in (Fig. 1) for identifying EGFR inhibitors was effective overall.

### Pharmacophore modelling and validation

A computational method entitled pharmacophore modeling is used in drug discovery to determine essential chemical characteristics or properties needed for a ligand to interact with a receptor (Hu et al. 2019). A crucial phase in pharmacophore modeling is pharmacophore query creation, and for this VLifeMDS (Molecular Design Suite) software was employed (VLife Sciences 2023). A group of 10 structurally diverse ligands in their bioactive conformation was subjected to docking and gain multiple conformations of each ligand. This step ensures ligand flexibility. A minimum of three pharmacophoric features were requested. Erlotinib was

employed as a reference compound and all 10 compounds with 10 conformations (a total of 100) were utilized for alignment purposes that aid to find common features which contribute to ligand binding with a receptor. The MolSign module in VLifeMDS provides tools for aligning small molecules based on their 3D pharmacophoric features. 30 Å tolerance limit was allowed when comparing two features across two molecules while 10 Å maximum distance was allowed between the two features (Panigrahi et al. 2020). The pharmacophore model was generated on the basis of 3 essential features (HAc:0 HAc:1 HDr:2) identified during alignment and further used for virtual screening of prepared database of benzofuran-1,2,3-triazole compounds to identify novel hits with improved binding affinity. The structures of FDA-approved compounds having benzofuran nucleus are given in (Supporting Figure S1). Pharmacophore common feature identifications in FDA-approved compounds are given in (Supporting Table S2). The pharmacophore model was validated via AUC curve (area under curve) and Enrichment Factor (EF) before screening to check the model's ability to predict active or inactive compounds from a dataset of both. For this download the decoy dataset from DUD (<https://dud.docking.org/>), a directory of useful decoys and active compounds from DrugBank using smiles of nucleus molecule of BENZ and generate a graph depicting AUC value and find EF for the top 1% and 20%. The resultant values are between 0 and 1. Values above 0.80 are considered significant as it depicts that the predicted pharmacophore

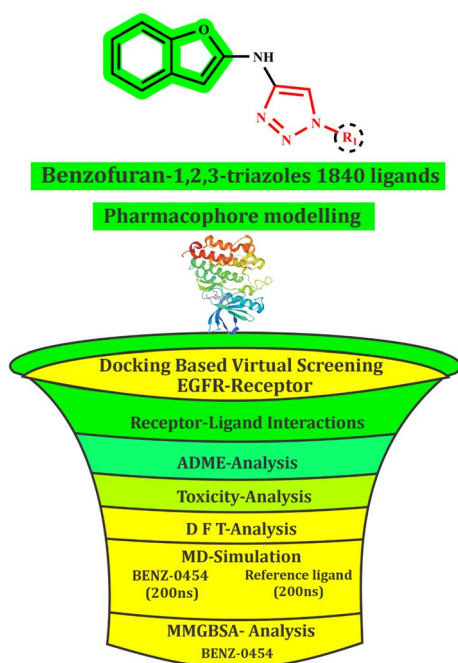


**Fig. 1** Scheme for Pharmacophore modeling and molecular docking-based virtual screening of benzofuran-1,2,3-triazole hybrids as potential inhibitors targeting EGFR in lung cancer

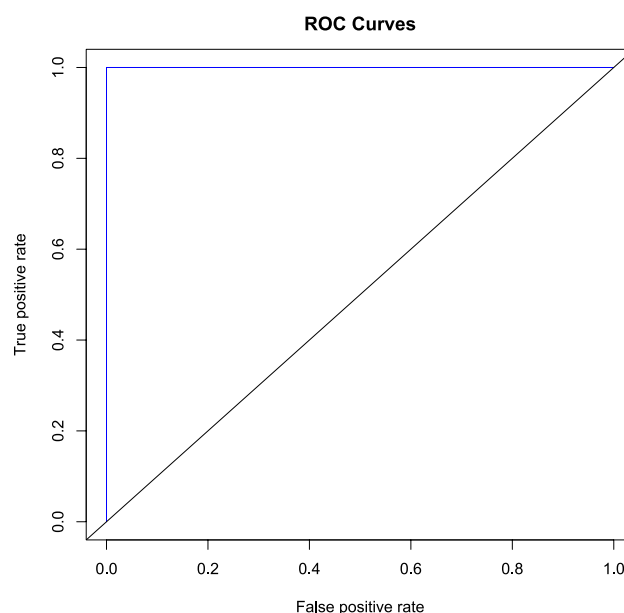


**Fig. 2** Pharmacophore validation via ROC curve where values range from 0 to 1 and higher values close to 1 considered good. Here blue line represented 1 AUC value while black horizontal line depicts 0.5 value which signifies random classification

model is good enough to further use for virtual screening of a prepared library of BENZ derivatives as shown in (Fig. 2).

## Molecular docking

Molecular docking is a computational method used in drug discovery to predict the binding of small molecules to a target protein (Stanzione et al. 2021). It is used to predict the binding mode, binding energy, and other thermodynamic and kinetic parameters of the interaction between a small molecule and a protein (Kontoyianni 2017). Molecular docking can be used in different stages of the drug discovery process, including Lead identification (Molecular docking can be used to identify new small molecules that have a high likelihood of binding to a specific target protein). Lead optimization (Molecular docking can be used to optimize the binding of a lead compound to a target protein by predicting the effects of small changes to the chemical structure of the compound on its binding properties) (Li et al. 2021). Virtual screening (Molecular docking can be used to screen large libraries of compounds to identify those that have the highest likelihood of binding to a specific target protein). Drug repurposing (Molecular docking can be used to identify new potential indications for existing drugs by predicting their binding to other target proteins) (Upadhyay et al. 2019). Molecular docking is a powerful computational tool that can be used to identify new drug candidates and to optimize the binding of existing drug candidates to target proteins (Pinzi and Rastelli 2019). To find the binding interactions of all the benzofuran-1,2,3-triazole hybrids in the active site of EGFR crystallographic receptor as anticancer target having (<https://www.rcsb.org/structure/4HJO>) (PDB ID: 4HJO) (Park et al. 2012). (Supporting Table S3) contains information on mutations, resolution, missing regions, and active state, before conducting molecular docking, the retrieved crystal structure was pre-processed to remove water and ions, and nonpolar hydrogens were combined. Then, the protein was processed for minimization and optimization through AutoDock Tool version 1.5.7 (<https://autodocksuite.scripps.edu/adt>) (Cosconati et al. 2010), bundled with the MGLTools package (<https://ccsb.scripps.edu/mgltools>) version 1.5.6 to add charges, and polar hydrogen atoms (Morris et al. 2009). Benzofuran-1,2,3-triazole hybrids were prepared in PyRx in which energy of all the ligands were minimised and converted to.pdbqt format (O'Boyle et al. 2011) The molecular docking was performed using PyRx virtual screening tool free version (<https://sourceforge.net/projects/pyrx>) (Dallakyan and Olson 2015). After completing the molecular docking, the resulting docking scores were saved in a.CSV file, indicating the affinity binding (Kcal/mol) of the output. The next step involved using PyMOL (version 2.5.4) to analyze the most favorable poses and their interactions (<http://www.pymol.org>) (Chaudhari and Li 2015). Utilizing

default docking algorithms, we set up grids with coordinates [X = 25.05, Y = 19.53, Z = 6.61] for (PDB ID: 4HJO) within the active site pocket. The grids' standard size enabled effective analysis. Among the benzofuran-1,2,3-triazole hybrids, those with the lowest binding energies displayed the most favorable interactions.

## ADME and drug likeliness analysis

ADME (Absorption, Distribution, Metabolism, and Excretion) in-silico analysis is a computational method for predicting the pharmacokinetic properties of a drug candidate (Paul Gleeson et al. 2011). This includes how well the drug is absorbed into the bloodstream, how it is distributed to different parts of the body, how it is metabolized by enzymes in the liver, and how it is excreted from the body (Wang et al. 2015). In-silico analysis is a cost-effective and efficient way to predict ADME properties and can help identify potential issues early in the drug development process before costly animal and human studies are conducted (Honorio et al.). A drug-likeness analysis is a computational method used in pharmaceutical research to predict the potential of a compound to be developed as a drug (Danielson et al. 2017). This analysis is based on the assessment of various chemical and physical properties of a compound, such as molecular weight, lipophilicity, and polar surface area, which are known to influence the pharmacokinetics, pharmacodynamics, and safety of a drug (Tian et al. 2015). Drug-likeness analysis can help identify compounds that are more likely to have favorable pharmacological properties and to be drug candidates (Jia et al. 2020). It can be done in-silico by using various software and databases that are available to predict these properties based on the chemical structure of the compound (Kurter et al. 2022). The virtually screened benzofuran-1,2,3-triazole hybrids acquired with the use of dock scores were then submitted to ADME analysis. SwissADME (<http://www.swissadme.ch>) (Daina et al. 2017) and ADMET 2.0 online servers (<https://admetmesh.scbdd.com>) tools accessed on 10 November 2022 (Xiong et al. 2021) were used to estimate drug-likeness and ADME features of benzofuran-1,2,3-triazole hybrids (Terstappen and Reggiani 2001).

## Toxicity-based screening

In-silico toxicity-based screening is a computational method for predicting the potential toxicity of a compound before it is tested in-vitro or in-vivo (Valerio 2009). It utilizes various computational tools, such as molecular docking, molecular dynamics simulations, and quantitative structure–activity relationship (QSAR) models, to predict the interactions between a compound and a target protein and to estimate the toxicity of the compound (Raies and Bajic 2016). In-silico

toxicity-based screening can provide a quick and cost-effective way to identify compounds that may have safety issues before they are tested in animal or human studies (Dearden 2003). This can save time and resources in the drug discovery process by reducing the number of compounds that need to be tested in-vivo (Daoud et al. 2021). Additionally, in-silico toxicity-based screening can also be used to identify potential side effects of a compound early on and to design safer compounds by predicting the toxicity of the compounds. This can help to increase the chances of successfully bringing a new drug to market by identifying compounds that are more likely to be safe and effective.

The assessment of benzofuran-1,2,3-triazole hybrids' effects and efficacy holds significant relevance in drug research and development. Understanding these aspects is critical as drug-induced toxicities in key organs, including the kidneys, brain, liver, and heart, account for about 75% of current drug retention and discontinuation cases (Cooper 2016). After conducting the ADME and drug likeliness analysis, specific benzofuran-1,2,3-triazole hybrids were chosen for toxicity prediction using in-silico tools. To assess toxicity, the OSIRIS property explorer was employed (<http://www.organic-chemistry.org/prog/peo>) tools accessed on 14 November 2022 (Sander et al. 2009) and ADMET 2.0 online servers (<https://admetmesh.scbdd.com>) tools accessed on 16 November 2022 (Xiong et al. 2021), were used to predict the toxicity features of the benzofuran-1,2,3-triazole hybrids.

### Density functional theory

Density Functional Theory (DFT) and similar methodologies are used to more precisely characterize a system's quantum mechanical properties. As a result, first-principles calculations have matured to the point that they can forecast a material's various properties with high accuracy and closely resemble experimental results. This theory also accurately predicts the nature of the interaction between molecular atomic orbitals. In conformity with experimental results, DFT theory accurately predicted reactivity and reaction process. M. Darvish Ganji and colleagues investigated drug release using carbon nanotubes (CNTs) and the DFT theory (Darvish Ganji et al. 2017). Using calculations based on fundamental principles, the investigation of many various pharmaceutical administration techniques might be accelerated and made more cost-effective. The advantages of the experiments make this a viable option. Scientists can optimize and relax their structures into the global minimum energy utilizing first-principles calculations and a wide range of known quantum mechanical theories, such as DFT, and their accompanying exchange–correlation functional basis sets. Scientists can now achieve this thanks to first-principles calculations, which is a big step forward. Scientists can learn more about the longevity of structures and whether they can

be found in nature or synthesized intentionally by investigating the imaginary frequencies of the infrared spectrum. This information should be available to the investigators. If a structure is discovered by theoretical calculations, there is an extremely slim possibility that it will ever be discovered in nature because naturally existent materials cannot have imaginary frequencies.

### Computational methodology (CM)

Density functional theory (DFT) was used to determine the electronic properties of molecules. The basis set 6-311G (d, p) was used with the hybrid correlation functional Becke's three-parameter Lee–Yang–Parr (B3LYP) (Gill et al. 1992). All computations were carried out using the quantum software Gaussian 16, Revision A. 03 (Frisch et al. 2016), simulation package on a high-performance computing cluster, and the results were shown using the GaussView 6.0 tool. We optimized the geometry of the molecules in order to find the lowest possible energy level and to get actual local minima at the same theoretical level. We used geometry optimization and frequency calculations to check for imaginary frequencies in our compounds, and when we didn't find any, it demonstrated that our compounds could be used and made in synthetic labs as well. We computed molecular electrostatic potential maps (MESP), frontier molecular orbitals (FMOs), and density of state (DOS) at the same B3LYP/6-311G\*\* theoretical level. All investigated compound's chemical structures and ground state geometry optimization are represented in (Fig. 3).

### Molecular dynamics simulation

Molecular dynamics (MD) simulation is a computational method used in drug discovery to study the dynamics of biomolecular systems, such as proteins and small molecules. MD simulation involves the use of mathematical models to simulate the interactions between the atoms in a biomolecular system over time. This allows researchers to study the behaviour of the system under different conditions, such as in the presence of different ligands or under different temperatures or pressure. MD simulations can be used to study the interactions between different proteins in a complex, which can provide insights into how drugs can modulate these interactions. The lead compound in contact with the receptor and STD complex were carried out for 200 ns MD simulation via Desmond software to analyze in the physiological conditions (Shaw Research 2023). Minimize energy of both systems (BENZ-0454 and STD complex), solvated by TIP3P water model in the orthorhombic box (10 Å × 10 Å × 10 Å) (Pandi et al. 2022) while the system was set up by system builder tool and neutralized by adding 0.15 M NaCl concentration. During MD simulation, the temperature of both

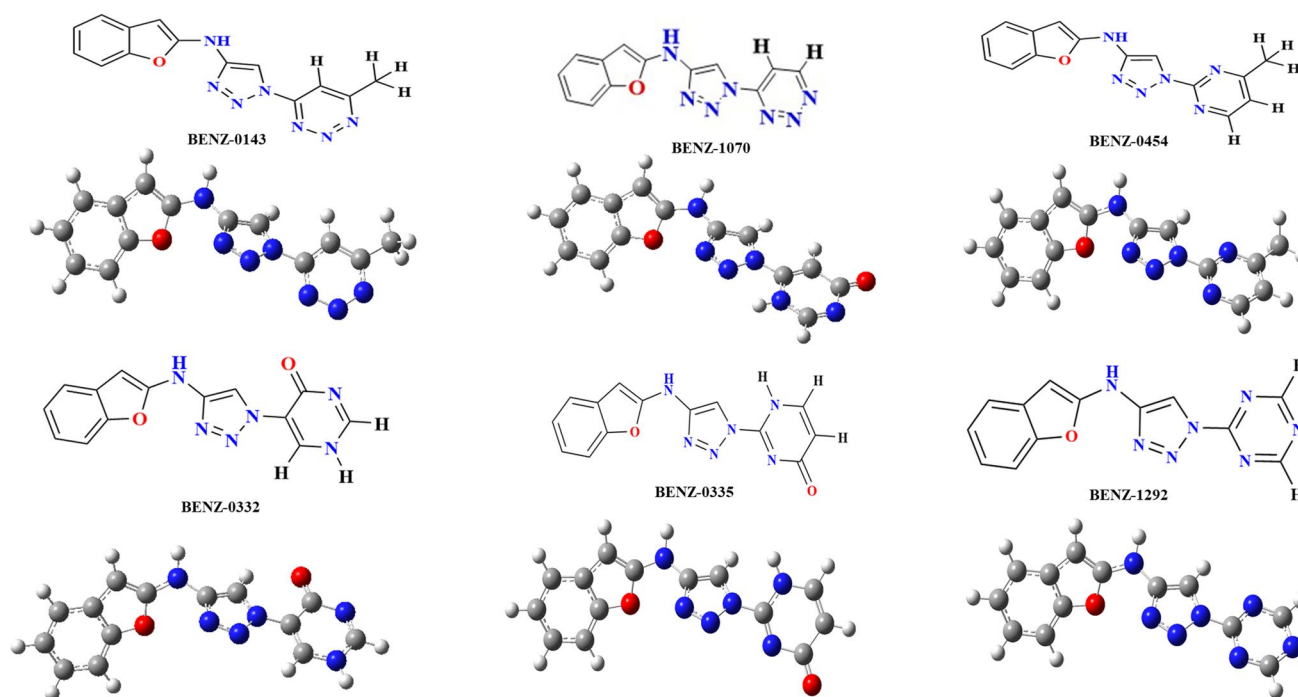


**Fig. 3** Showing ChemDraw chemical structures and ground state geometry optimization at DFT/B3LP/6-311G\*\* level of theory of best six benzofuran-1,2,3-triazole hybrids

complexes gradually increased from 200 to 250 K and then 300 K with 1 atm pressure in order to stabilize the system. The interaction between protein and ligand was examined via the simulation interaction diagram tool (Rasheed et al. 2021). The MD simulation was successfully conducted using an Intel Core i9-12900KF processor, 128 GB of RAM, and MSI GeForce RTX 3080 Ti GPU on a custom liquid-cooling desktop running Ubuntu 22.04.1 LTS.

### MMGBSA analysis

MMGBSA (Molecular Mechanics Generalized Born Surface Area) is a computational method that is used to estimate the binding free energy between a small molecule, such as a drug, and a target protein that allows the calculation of the relative stability of different protein–ligand complexes and differentiate binders and non-binders (Genheden and Ryde 2015). The energy of the system is calculated using molecular mechanics force fields, and the interactions between the protein and the ligand are taken into account. MMGBSA analysis was executed for both BENZ-0454 and STD compounds fit in target protein EGFR (PDB ID: 4HJO) by Prime Schrodinger which calculates the energy of optimized free receptors, free ligand, and a complex of the ligand fit protein (Jacobson et al. 2004). The total of the gas-phase energy, solvation-free energy, and entropic contributions was computed using

the MMGB/SA method to get the absolute binding free energies of both complexes. By breaking down the total binding free energy into its constituent parts including coulomb, covalent, lipophilic, H-bond, selfcount (Self contact correction), packing (pi-pi packing), Solv GB (Generalized Born electrostatic solvation energy), and van der Waals. This helps us to understand the complicated binding process more thoroughly (Zhang et al. 2017).  $\Delta G_{\text{bind}}$  (binding free energy) of protein–ligand complex determined using Eq. (1).

$$\Delta G_{\text{bind}} = \Delta E_{\text{vdw}} + \Delta E_{\text{ele}} + \Delta E_{\text{GB}} + \Delta E_{\text{SA}} - T\Delta S \quad (1)$$

According to this equation, the total binding free energy of the complex is  $\Delta G_{\text{bind}}$ . While  $\Delta E_{\text{vdw}}$ ,  $\Delta E_{\text{ele}}$ ,  $\Delta E_{\text{GB}}$ ,  $\Delta E_{\text{SA}}$ , and  $T\Delta S$  represent van der Waals, Coulombic energy, generalized born electrostatic solvation free energy (polar energy), nonpolar (solvent accessible surface area), and conformational entropy respectively.

MMGBSA analysis provides information about the binding free energy, which is the difference in energy between the bound and unbound states, and the contributions of the different energy components to the overall binding free energy. This information can be used to identify the key interactions between the protein and the ligand and to predict the binding affinity of the ligand to the protein.

## Results and discussion

### Pharmacophore screening

A comprehensive distance-based pharmacophore model was generated via VLifeMDS using a training dataset of bioactive compounds known as EGFR tyrosine kinase inhibitors. MolSign module uses a robust VLifeEngine algorithm to select 3D pharmacophoric features on the basis of several flexible alignments of these training dataset compounds and detect outliers. The selected query

contains 3 features (2 hydrogen bond acceptors (Hac) and 01 donor (HDr) shown in blue and green colors respectively) necessary to inhibit the target protein as shown in (Fig. 4) while the distance between all three features was 6.179 (Hac1–HDr3), 2.410 (Hac1–Hac2) and 5.041 Å (Hac2–HDr3) given in (Table 1). Pharmacophore validated and display excellent results. AUC value of 1 shows that the predicted model is able to select active compounds instead inactive and can be further used for screening. Figure 2 shows an AUC graph where the blue line shows the pharmacophore model's efficiency. EF for top 1% is 27 and for top 20% is 4.5 indicating that pharmacophore is

**Fig. 4** (A) Pharmacophore modelling hypothesis of FDA approved compounds which have EGFR kinase inhibitory activity along selected features (shown in sphere) and distances. (B) 20 Hit compounds with distance-based Pharmacophore features in the benzofuran-1,2,3-triazole hybrids

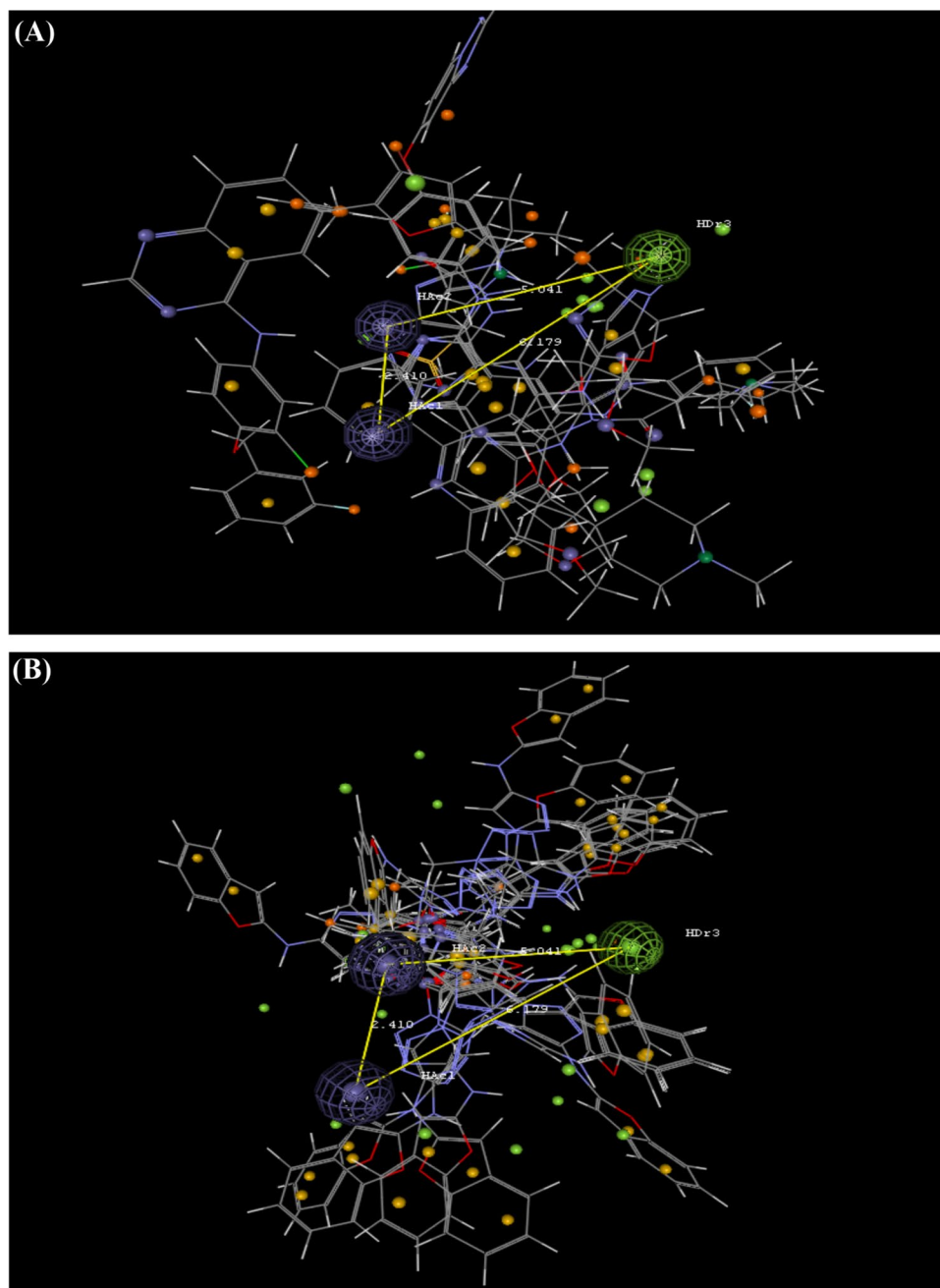


**Table 1** Benzofuran-1,2,3-triazole hybrid's pharmacophoric features along their distances in angstrom

Sr.no	Pharmacophore features	Distance (Å)
1	Hac1-HDr3	6.179
2	Hac1-Hac2	2.410
3	Hac2-HDr3	5.041

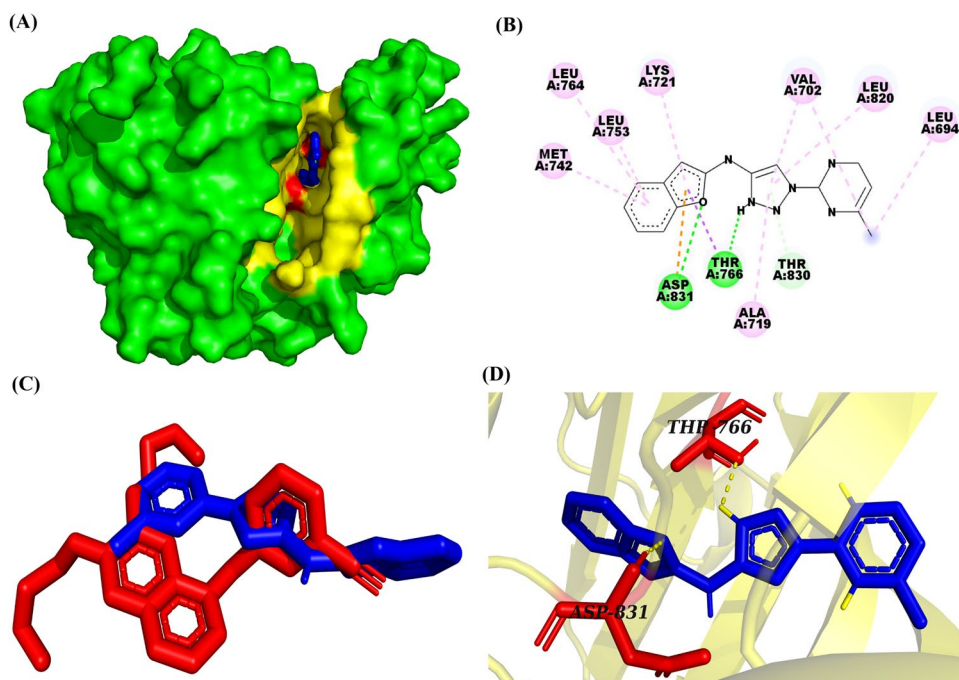
able to immediately selects most of the active compounds from a dataset of both active and inactive. Therefore, the predicted pharmacophore query was further used to screen the library of 1841 Benzofuran-1,2,3-triazole derivatives. Resultantly, 20 hits were obtained that would be further used for molecular docking to predict novel lead compounds. (Fig. 4B) depicts 20 hit compounds after screening with their labeled pharmacophoric features and distance. The pharmacophore-based screening results of benzofuran-1,2,3-triazole are given in (Supporting Table S3).

### Docking based virtual screening

A molecular docking process was performed for the designed benzofuran-1,2,3-triazole hybrids to investigate and compare the binding energies and interactions with the selected EGFR target protein. EGFR consists of a conserved catalytic kinase domain consisting of a smaller N-lobe (comprising 5 beta strands and conserved alpha helix) and a larger C-loob (comprising 5 alpha helices) (Kumar et al. 2008) (Martin-Fernandez et al. 2019). The affinity scores of the top

six benzofuran-1,2,3-triazole hybrids BENZ-0454, BENZ-0143, BENZ-1292, BENZ-0335, BENZ-0332, and BENZ-1070 for (PDB ID: 4HJO) was observed as  $-10.2$ ,  $-10$ ,  $-9.9$ ,  $-9.8$ ,  $-9.7$ ,  $-9.6$ , while for reference molecule affinity score  $-7.9$  kcal/mol respectively. Ligand efficiency (LE) for BENZ-0454, BENZ-0143, BENZ-1292, BENZ-0335, BENZ-0332, BENZ-1070, and reference ligand (erlotinib) was found to be, 0.635, 0.622, 0.645, 0.61, 0.604, 0.626, and 0.373 respectively. Ligand Lipophilic Efficiency (LLE) ranged between 5 to 8.7 while Ligand Efficiency Lipophilic Price (LELP) are in between 1.6 and 8.0. BENZ-0454 demonstrated the lowest binding affinity as compared to other benzofuran-1,2,3-triazole hybrids. The docking poses of the BENZ-0454 with the selected target (PDB ID: 4HJO) were analyzed with 2D interactions as shown in (Fig. 5). The residues Thr766 and Asp831 were observed to be forming hydrogen bonds with BENZ-0454. It was observed that the residues Asp831 and Thr766 were forming hydrogen bonds with BENZ-0143. BENZ-1292 was observed to exhibit hydrogen bonding with residues Asp831 and Thr766. The presence of hydrogen bonds between BENZ-0335 and residues Asp831, and Thr766 was detected. It was observed that BENZ-0332 was forming hydrogen bonds with residue Asp831. The residues Asp831 and Arg817 were observed to be forming hydrogen bonds with BENZ-1070. The hydrogen bonding between the reference ligand and residues Asp831, Cys773, and Met769 of the EGFR-TKD receptor (PDB ID: 4HJO) was observed with a binding energy of  $-7.9$  kcal/mol. The hydrogen bonding interaction plays a critical role in improving the interaction with the active sites of the receptor. In the reference molecule, only three hydrogen

**Fig. 5** (A) Surface mapping of benzofuran-1,2,3-triazole hybrid BENZ-0454 blue color in the receptor cavity of EGFR (PDB ID:4HJO) (B) Showing 2D interaction view of benzofuran-1,2,3-triazole hybrid BENZ-0454 with the EGFR receptor (PDB ID:4HJO). (C) Representing superimposed view of reference ligand in red color and benzofuran-1,2,3-triazole hybrids BENZI-0660 blue color in the receptor cavity of EGFR (D) Benzofuran-1,2,3-triazole hybrid BENZ-0454 in the blue color showing polar contacts with the residues of EGFR (PDB ID:4HJO)



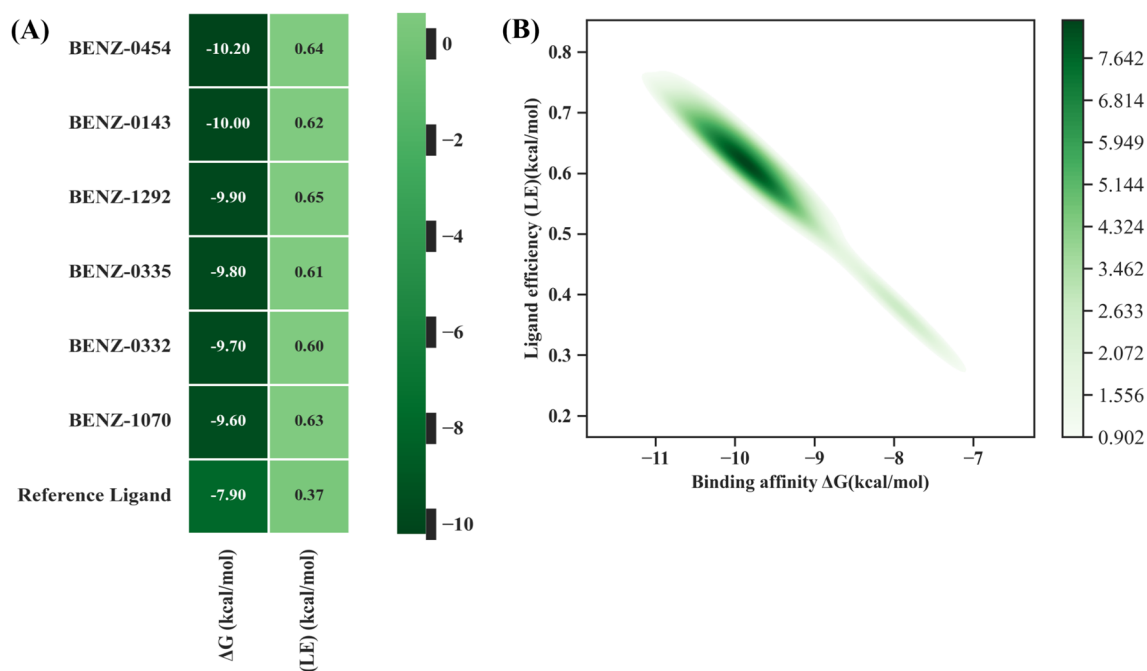


bonding interactions are formed with the residues Asp831, Cys773, and Met769. In the designed ligand BENZ-0454 there are two hydrogen bonding interactions found with the following residues like Thr766, and Asp831. To check the target selectivity of the best hit compound (BENZ-0454), docked with inactive state of EGFR (PDB ID: 3W32, 5Y9T) and results depict that the hit compound didn't make interaction with active site residues as claimed with active EGFR binding. Figure 6 depicts the correlation between binding affinity and ligand efficiency. Ligand interaction with residues Thr766 is found to be new when it is compared with the reference molecule interactions as shown in Table 2. The docking results of all the screened ligands can be seen in the supporting (Supporting Table S4).

### ADME analysis initial of the hit compounds

After conducting docking-based virtual screening, the ligands BENZ-0454, BENZ-0143, BENZ-1292, BENZ-0335, BENZ-0332, and BENZ-1070 were shortlisted for ADME analysis. The selection criteria were their top dock scores with the EGFR-TKD receptor, a crucial anticancer target (PDB ID: 4HJO). The molecular structure of BENZ-0454 includes three rotatable bonds, five H-bond acceptors, and one H-bond donor. Moreover, it scored a synthetic accessibility value of 3.18 and a bioavailability score of 0.55. Interestingly, the ligand demonstrated high

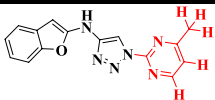
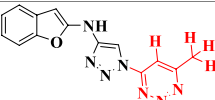
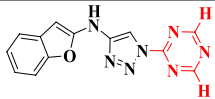
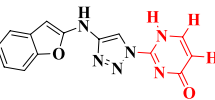
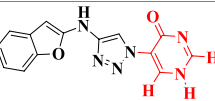
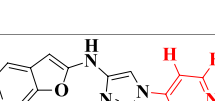
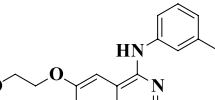
GI absorption while showing no permeation through the blood–brain barrier (BBB). In the case of BENZ-0143, there are three rotatable bonds, along with six H-bond acceptors and one H-bond donor. The ligand's synthetic accessibility score is 3.14, and it has a bioavailability score of 0.55. Remarkably, BENZ-0143 displays high GI absorption and does not permeate the BBB. The analysis of BENZ-1292 reveals the presence of three rotatable bonds, six H-bond acceptors, and one H-bond donor. Furthermore, the ligand's synthetic accessibility score is 3.16, and it has a bioavailability score of 0.55. Interestingly, BENZ-1292 demonstrates high GI absorption and does not permeate the BBB. In the case of BENZ-0335, there are three rotatable bonds, along with five H-bond acceptors and two H-bond donors. The ligand's synthetic accessibility score is 3.15, and it has a bioavailability score of 0.55. Remarkably, BENZ-0335 displays high GI absorption and does not permeate the BBB. BENZ-0332 was found to have three rotatable bonds, five H-bond acceptors, and two H-bond donors in its structure. The ligand's synthetic accessibility score is 3.26, and it has a bioavailability score of 0.55. Notably, it demonstrates high GI absorption and does not permeate the BBB. BENZ-1070 exhibits three rotatable bonds, six H-bond acceptors, and one H-bond donor. It received a synthetic accessibility score of 3.1 and a bioavailability score of 0.55. Notably, the ligand demonstrates high GI absorption while showing no permeation through the BBB. The reference ligand was



**Fig. 6** (A) Showing comparison of Binding affinity and Ligand efficiency (LE) of best six benzofuran-1,2,3-triazole hybrids with the reference ligand on the basis of docking score with the EGFR (PDB

ID: 4HJO) (B) Representing correlation between Binding affinity and Ligand efficiency (LE) of best hit benzofuran-1,2,3-triazole hybrid BENZ-0454

**Table 2** Molecular docking analysis of the best six benzofuran-1,2,3-triazole hybrids with epidermal growth factor receptor tyrosine kinase domain (PDB ID: 4HJO)

Ligand	Designed ligand $\Delta G$ (kcal/mol)	Ligand efficiency (LE) (kcal/mol)	Ligand Lipophilic Efficiency (LLE)	Ligand Efficiency Lipophilic Price (LELP)	H-Bond interaction residues (Distance in Å and angle in degree)	Vander Waal's interacting residues	Pi-Alkyl/Pi-Pi interacting residues (Å)
 <b>BENZ-0454</b>	-10.2	0.635	7.3	4.5	Thr 766 (2.4) (111.5°), Asp 831 (2.3) (103.3°)	Met 769, Leu 768, Gly 772, Thr 830, Leu 834, Phe 832, Cys 751	Met 742 (4.8), Leu 753 (4.7), Leu 764 (5.4), Lys 721 (5.1), Leu 820 (5.2), Ala 719 (4.3), Val 702 (4.9)
 <b>BENZ-0143</b>	-10	0.622	7.08	4.6	Asp 831 (2.2) (103.4°), Thr 766 (2.5) (108.8°)	Thr 830, Leu 834, Cys 751, Phe 832, Leu 764, Met 769, Gly 772, Cys 773	Leu 694 (5.1), Leu 820 (3.7, 5.3), Val 702 (4.6, 4.8), Ala 719 (4.4, 4.8), Lys 721 (5.2), Met 742 (4.7), Leu 753 (4.7)
 <b>BENZ-1292</b>	-9.9	0.645	7.5	3.6	Asp 831 (2.1) (73.2°), Thr 766 (2.5) (113.8°)	Cys 773, Leu 694, Gly 772, Leu 768, Met 769, Thr 830, Cys 751, Phe 832	Met 742 (4.7), Leu 764 (5.3), Lys 721 (5.2), Leu 834 (5.4), Leu 753 (4.6), Val 702 (5), Ala 719 (4.5), Leu 820 (5.2)
 <b>BENZ-0335</b>	-9.8	0.61	7.45	3.8	Asp 831 (2.2) (102.7°), Thr 766 (2.4) (132.1°)	Cys 773, Leu 694, Met 769, Leu 768, Gly 772, Thr 830, Leu 834, Phe 832,	Ala 719 (4.7), Val 702 (4.8), Leu 820 (5.1), Lys 721 (5.1), Met 742 (4.8)
 <b>BENZ-0332</b>	-9.7	0.604	8.7	1.65	Asp 831 (2.1, 2.6) (110.1°, 96.5°)	Gly 772, Leu 694, Ala 719, Thr 766, Cys 751, Phe 832, Cys 773, Arg 817, Thr 830, Leu 764	Lys 721 (4.9, 5.2), Val 702 (4.7), Leu 820 (5.4), Met 742 (4.8), Leu 834 (5.3), Leu 753 (4.7)
 <b>BENZ-1070</b>	-9.6	0.626	7.39	3.5	Asp 831 (2.9) (100.9°), Arg 817 (2.2) (132.2°)	Cys 773, Asn 818, Leu 764, Phe 832, Cys 751, Thr 830	Val 702 (4.7), Leu 820 (5.4), Lys 721 (5), Leu 834 (5.3), Met 742 (4.9), Leu 753 (4.8)
 <b>Reference ligand</b>	-7.9	0.373	5.0	8.0	Asp 831 (2.2) (145.8°), Met 769 (1.90) (124.6°)	Thr 830, Thr 766, Leu 753, Leu 768, Leu 694, Gly 772, Asp 776, Gly 695, Leu 820, Gln 767,	Leu 834 (4.4), Lys 721 (4.2), Val 702 (4, 4.8), Ala 719 (4.8), Leu 764 (5.2)

found to have ten rotatable bonds, six H-bond acceptors, and one H-bond donor in its structure. The ligand's synthetic accessibility score is 3.19, and it has a bioavailability score of 0.55. Notably, it illustrates high GI absorption and permeates the BBB.

BENZ-0454's ADME profiles were found to be satisfactory, characterized by three rotatable bonds, five H-bond acceptors, and one H-bond donor. The ligand's synthetic accessibility score is 3.18, and it has a bioavailability score of 0.55. Notably, it exhibited high GI absorption and did not permeate the BBB. Figure 7 displays the results of ADME analysis conducted on the best six ligands. The compounds that satisfied Lipinski's rule of five, had high gastrointestinal retention, and exhibited zero PAINS alerts were shortlisted for further screening. The compounds listed in Table 3 met these requirements and had synthetic accessibility scores of less than five.

### Toxicity-based screening

After performing the ADME analysis, the subsequent step was to analyse the toxicity profile of the ligands that underwent virtual screening. The designed ligands BENZ-0454, BENZ-0143, BENZ-1292, BENZ-0335, BENZ-0332, and BENZ-1070 were selected for toxicity profile prediction on the basis of docking score with EGFR-TKD receptor as anticancer target (PDB ID: 4HJO). BENZ-0454 did not demonstrate any tumorigenic risk, mutagenic potential, or irritancy. However, mild reproductive effects were observed. There is no evidence of tumorigenicity or irritancy associated with

BENZ-0143. However, a mild risk of mutagenic indication was observed, and no adverse effects on reproduction were noted. There is no risk of tumorigenicity, mutagenicity, or reproductive toxicity associated with BENZ-1292, but it has a mild irritant property. BENZ-0335 showed no tumorigenic potential, mutagenic activity, or adverse effects on reproduction, and it is non-irritating. There is a mild risk of tumorigenicity associated with BENZ-0332, but no indications of mutagenicity or adverse effects on reproduction or irritancy were observed. There is no evidence of tumorigenicity, mutagenicity, or irritancy associated with BENZ-1070, and no effects on reproduction were noted. The use of erlotinib as a reference ligand has been connected with various side effects and toxicities, including stabbing chest pain, a sensation of pins and needles, numbness, or pain in the hands, arms, feet, or legs, tingling, burning, rash, fever, difficulty breathing, diarrhea, and coughing. The reference ligand was compared with the designed ligands and finally, BENZI-0660 had acceptable toxicity profiles for all of them, and therefore was chosen as the final hit compound. The toxicity profile of the best six ligands is presented in (Fig. 8). Six symbols are used to represent the prediction probability values, with ranges assigned as follows: '-' (0–0.1), '- ' (0.1–0.3), '- ' (0.3–0.5), '+ ' (0.5–0.7), '+ +' (0.7–0.9), and '+ + +' (0.9–1.0) as shown in Table 4.

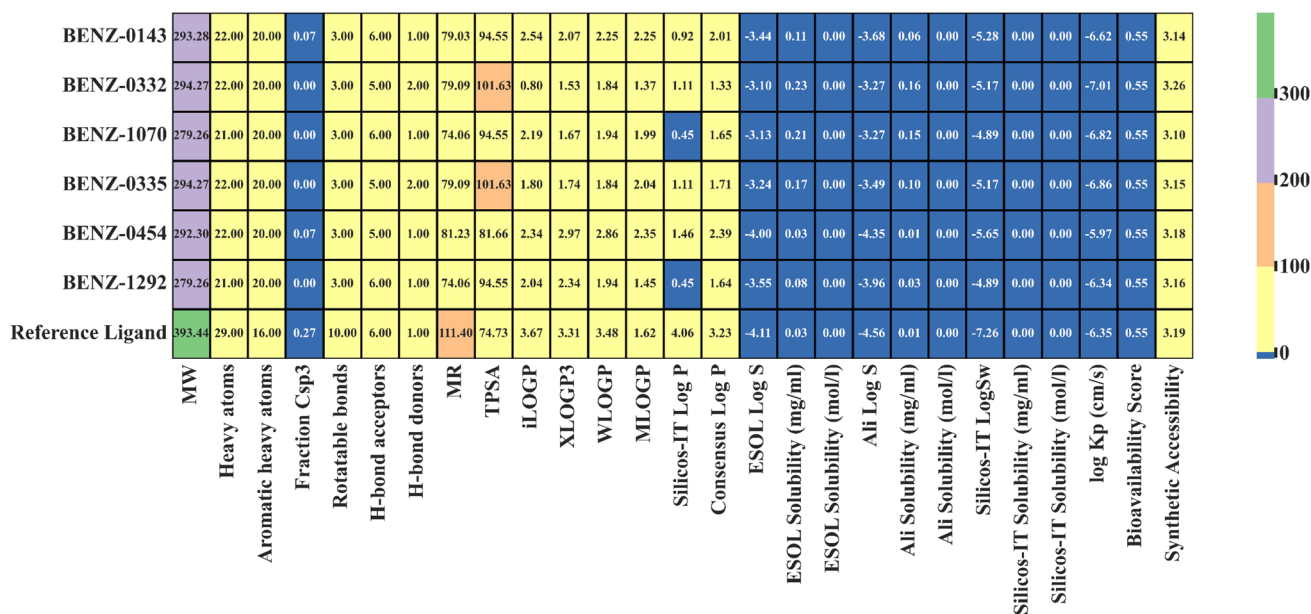


**Fig. 7** Showing ADME analysis for the best six benzofuran-1,2,3-triazole hybrids and comparison with reference ligand selected on the basis of docking score

**Table 3** Chemical absorption, distribution, metabolism, and excretion (ADME) properties of the benzofuran-1,2,3-triazole hybrids

Ligand	BENZ-0143	BENZ-0332	BENZ-1070	BENZ-0335	BENZ-0454	BENZ-1292	Reference ligand
MW	293.28	294.27	279.26	294.27	292.3	279.26	393.44
Heavy atoms	22	22	21	22	22	21	29
Aromatic heavy atoms	20	20	20	20	20	20	16
Fraction Csp <sup>3</sup>	0.07	0	0	0	0.07	0	0.27
Rotatable bonds	3	3	3	3	3	3	10
H-bond acceptors	6	5	6	5	5	6	6
H-bond donors	1	2	1	2	1	1	1
MR	79.03	79.09	74.06	79.09	81.23	74.06	111.4
TPSA	94.55	101.63	94.55	101.63	81.66	94.55	74.73
iLOGP	2.54	0.8	2.19	1.8	2.34	2.04	3.67
XLOGP <sub>3</sub>	2.07	1.53	1.67	1.74	2.97	2.34	3.31
WLOGP	2.25	1.84	1.94	1.84	2.86	1.94	3.48
MLOGP	2.25	1.37	1.99	2.04	2.35	1.45	1.48
Silicos-IT Log P	0.92	1.11	0.45	1.11	1.46	0.45	4.06
Consensus Log P	2.01	1.33	1.65	1.71	2.39	1.64	3.2
ESOL Log S	-3.44	-3.1	-3.13	-3.24	-4	-3.55	-4.11
ESOL Class	Soluble	Soluble	Soluble	Soluble	Soluble	Soluble	Moderately soluble
Ali Log S	-3.68	-3.27	-3.27	-3.49	-4.35	-3.96	-4.56
Ali Class	Soluble	Soluble	Soluble	Soluble	Moderately soluble	Soluble	Moderately soluble
Silicos-IT Log Sw	-5.28	-5.17	-4.89	-5.17	-5.65	-4.89	-7.26
Silicos-IT class	Moderately soluble	Moderately soluble	Moderately soluble	Moderately soluble	Moderately soluble	Moderately soluble	Poorly soluble
GI absorption	High	High	High	High	High	High	High
BBB permeant	No	No	No	No	No	No	Yes
Pgp substrate	No	No	No	No	No	No	No
CYP1A2 inhibitor	Yes	No	Yes	No	Yes	No	Yes
CYP2C19 inhibitor	Yes	No	Yes	No	Yes	Yes	Yes
CYP2C9 inhibitor	No	No	No	No	No	No	Yes
CYP2D6 inhibitor	No	No	No	No	No	No	Yes
CYP3A4 inhibitor	No	No	No	No	No	No	Yes
log Kp (cm/s)	-6.62	-7.01	-6.82	-6.86	-5.97	-6.34	-6.35
Lipinski violations	0	0	0	0	0	0	0
Ghose violations	0	0	0	0	0	0	0
Veber violations	0	0	0	0	0	0	0
Egan violations	0	0	0	0	0	0	0
Muegge violations	0	0	0	0	0	0	0
Bioavailability Score	0.55	0.55	0.55	0.55	0.55	0.55	0.55
PAINS alerts	0	0	0	0	0	0	0

**Table 3** (continued)

Ligand	BENZ-0143	BENZ-0332	BENZ-1070	BENZ-0335	BENZ-0454	BENZ-1292	Reference ligand
Brenk alerts	0	0	0	0	0	0	1
Lead likeness violations	0	0	0	0	0	0	2
Synthetic Accessibility	3.14	3.26	3.1	3.15	3.18	3.16	3.19

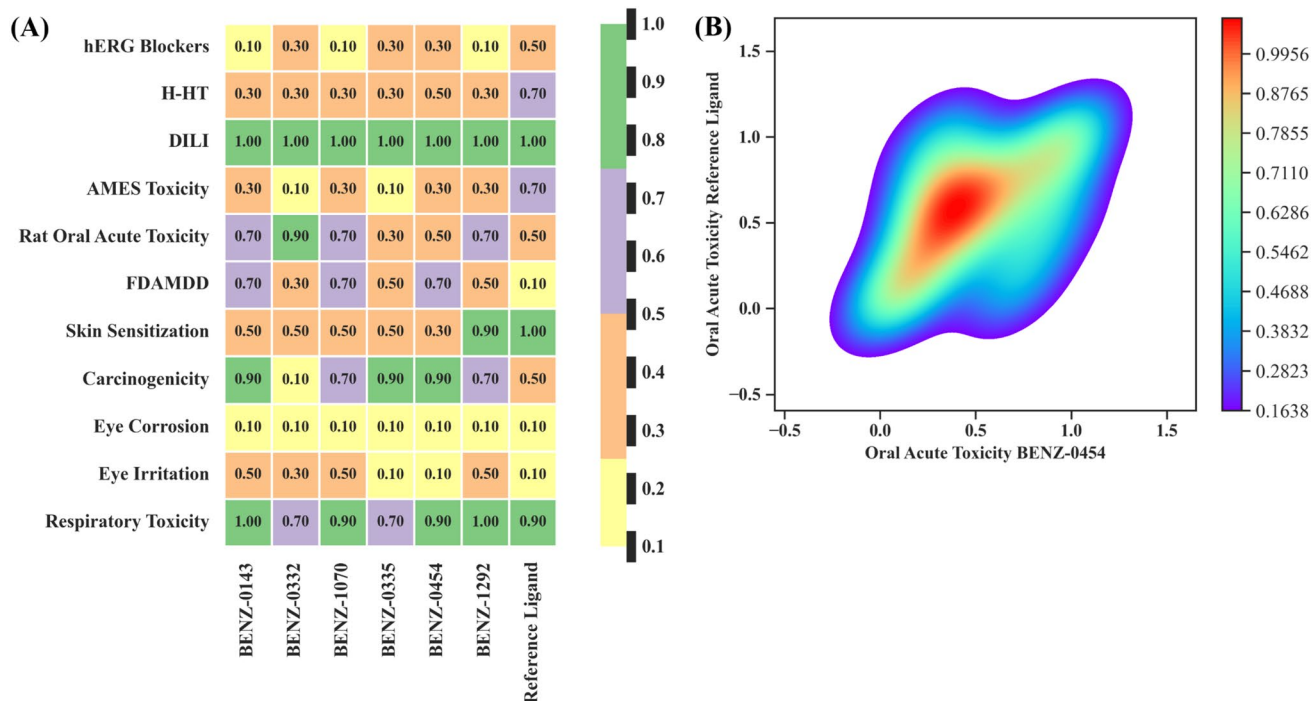


**Fig. 8** (A) Showing several toxicity parameters of best six benzofuran-1,2,3-triazole hybrids and comparison with the reference ligand. (B) Representing correlation between toxicity parameters of best hit benzofuran-1,2,3-triazole hybrids BENZ-0454 and reference ligand

## Density functional theory (DFT)-analysis

### Frontier molecular orbitals (FMOs)

The quantum method of density functional theory is commonly used in in-silico studies. Understanding the pharmacological effect of the chemicals requires an analysis of their electronic characteristics. The transition from the ground state to the first excited state can be best represented by a single excitation of an electron from the highest occupied molecular orbital (HOMO) to the lowest unoccupied molecular orbital (LUMO), as evidenced by a study of the wave function. The reactive properties of the phytochemicals were investigated using DFT analysis (Abbas et al. 2022b). As part of the DFT analysis, a code estimated the HOMO and LUMO energies of the molecules. Charge transfer within a molecule has been studied using HOMO and LUMO levels and their electron density regions are shown in Fig. 9.

The band energy gaps were used to determine the reactivity of the compounds. Because of the various LUMO and HOMO energies of the ligands, all of the complexes studied had varying band energy gaps. The computed gap energies were evaluated to determine the reactivity of the compounds. When the energy gap of a compound increases, its reactivity drops, and vice versa (Mohammadi et al. 2022). The small band energy gap range observed in this investigation is suggestive of the compounds' high reactivity (3.238–3.870 eV). Among our tailored compounds, BENZ-0143 has the smallest energy gap while BENZ-0335 has the largest. Reducing the BENZ-0143 molecule energy gap boosts its chemical activity. Compounds having a lower band energy gap are more reactive, as the LUMO and HOMO are critical for charge transfer during a chemical reaction, according to the literature. The energy level of a molecule can describe both its electrophilic and nucleophilic properties (Abbas et al. 2022a).

**Table 4** Toxicity prediction of the best six benzofuran-1,2,3-triazole hybrids

Ligand	BENZ-0143	BENZ-0332	BENZ-1070	BENZ-0335	BENZ-0454	BENZ-1292
hERG blockers	---	-	---	-	-	---
H-HT	-	-	-	-	-	-
DILI	+++	+++	+++	+++	+++	+++
AMES toxicity	-	---	-	---	-	-
Rat oral acute toxicity	+	++	+	-	-	+
FDAMDD	+	-	+	-	+	-
Skin sensitization	-	-	-	-	-	++
Carcinogenicity	++	---	+	++	++	+
Eye corrosion	---	---	---	---	---	---
Eye irritation	-	-	-	---	---	-
Respiratory toxicity	+++	+	++	+	++	+++
Mutagenic	Mild risk	No indication	No indication	No indication	No indication	No indication
Tumorigenic	No risk	Mild risk	No risk	No risk	No risk	No risk
irritant	No	No	No	No	No	Yes
Reproductive effects	No effect	No risk	No effect	No risk	Mild risk	No risk

The prediction probability values are converted into six symbols based on their range: 0–0.1 (represented as '---'), 0.1–0.3 ('-'), 0.3–0.5 ('-'), 0.5–0.7 ('+'), 0.7–0.9 ('++'), and 0.9–1.0 ('+++')

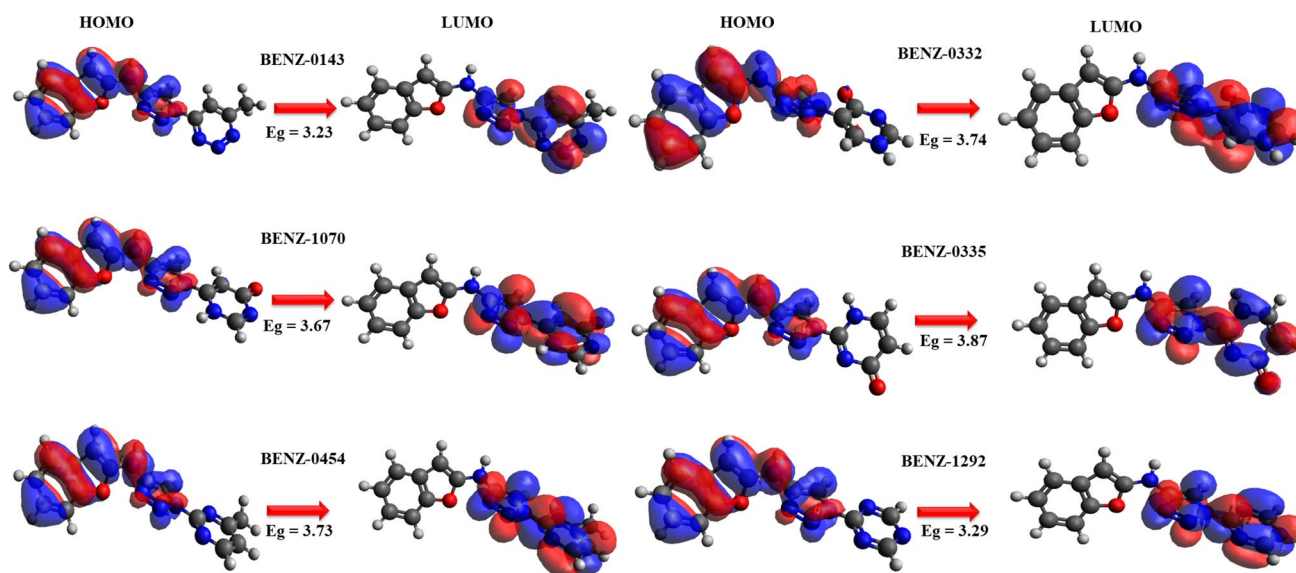


**Fig. 9** HOMO–LUMO distributions of electron density regions at B3LYP/6-31G\*\* level of theory. Red and violet show HOMO, while red and cyan show LUMO. These colors indicating which areas have the most electrons. After discussing about HOMO, LUMO, and

global reactivity descriptors in detail, it can be concluded that benzofuran-1,2,3-triazole hybrids BENZ-0454 seems to work best as an inhibitors because it takes up more space on the HOMO side

### Local and global reactivity descriptors

The density-functional theory (DFT) is an essential tool for determining the chemical reactivity of compounds by using various theories, such as Koopman's theorem regarding HOMO and LUMO energy levels, ionization potential (IP), and electron affinity (A) respectively Eqs. (2–7).

$$IP = -E_{HOMO} \text{ and } EA = -E_{LUMO} \quad (2)$$

As a result, different global reactivity descriptors like chemical hardness ( $\eta$ ), softness (S), electronegativity (X), chemical potential ( $\mu$ ), and electrophilicity index ( $\omega$ ) can be derived using the Eq. (2).

$$\eta = \frac{A + IP}{2} \quad (3)$$

$$s = \frac{1}{\eta} \quad (4)$$

$$\mu = \frac{A - IP}{2} \quad (5)$$

$$\omega = \frac{\mu^2}{2\eta} \quad (6)$$

$$x = -\mu \quad (7)$$

The global hardness ( $\eta$ ) of a molecule is defined as its resistance to changes in its electron configuration. The harness and aromaticity are related to one another in terms of the aromaticity of the number of unsubstituted compounds and the molecule's ability to arrange itself as hard as possible. Softness ( $S$ ) is the reverse of global hardness. Based on the HOMO–LUMO energy gap, local hardness indicates intermolecular reactivity; as the energy gap increases, reactivity decreases, and compounds with less reactivity are referred to as hard, whereas soft compounds have a smaller energy gap and are more polarization due to chemical changes. Electrophilicity ( $\omega$ ) is affected by two factors: the pace of electron transfer, the electrophile's ability to gain more electronic charge, and the degree to which it is unwilling to exchange electronic charge with its environment. The electrophilicity index ( $\omega$ ) plays a significant role in drug toxicity because it provides an estimation of the biological activity of pharmacological compounds based on their molecular reactivity and selectivity. More electron transport from the donor fragment to the acceptor side results in a higher global electrophilic index ( $\omega$ ). The more negative the chemical potential ( $\mu$ ) values of compounds are, the less they decompose into elements. In our investigated compounds, chemical potential ( $\mu$ ) values are BENZ-0143 (−4.060), BENZ-0332 (−3.693), BENZ-0333 (−3.890), BENZ-0335 (−3.750), BENZ-0335 (−3.742), and BENZ-1292 (−4.014), respectively. Due to low polarized, the chemical hardness ( $\eta$ ) measured from the HOMO–LUMO energy gap exhibits significant resistance to the deformation of the electronic cloud under small chemical changes. BENZ-0335 has higher global hardness ( $\eta$ ) values in our compounds, which indicates that it exhibits the least polarisation upon accepting chemical alterations. The global softness ( $S$ ) values of all tailored compounds are given as BENZ-0143 (0.617), BENZ-0332 (0.534), BENZ-0333 (0.544), BENZ-0335 (0.515), BENZ-0335 (0.534), and BENZ-1292 (0.616), respectively in the Table 5. Due to its high chemical potential ( $\mu$ ), the

compound BENZ-0143 (5.090) exhibits the greatest electrophilicity index ( $\omega$ ) value, which is an indication of nucleophilicity power.

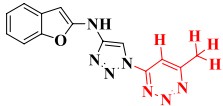
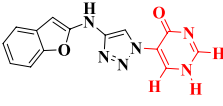
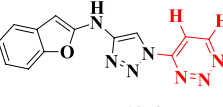
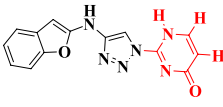
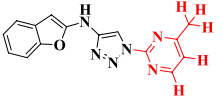
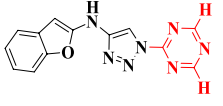
### Molecular electrostatic potential (MEP)

Molecular electrostatic potential maps (MEP) were created from the optimized geometry at the B3LYP/6-311G\*\* level so that the reactive sites of compounds may be anticipated in terms of electrophilic and nucleophilic reactions, how the different geometries interact with each other as well as the investigation of hydrogen bond interactions. By utilizing color coding to locate the negative, positive, and neutral electrostatic potential maps, these MEP maps are used to determine the physicochemical properties of the compounds that have been under investigation. They are helpful in locating the reactive regions where nucleophiles and electrophiles can attack and interact with the target molecule. When using color coding, the red color represents the electrostatic potentials that are the most negative, blue represents the electrostatic potentials that are the most positive, and green is used to highlight the sides of examined compounds that have zero potential. Electrophilic reactivity was associated with the components that possessed a negative charge, whereas nucleophilic reactivity was associated with the components that possessed a positive charge. The potential of the colors decreases from red to orange to yellow to green to blue. The maximum potential is found in the color red. Isosurfaces, which are shown in the MEP maps that show where there are strong concentrations of electrons, can be found on these maps (Fig. 10). A value of 0.002 a.u. can be assigned to each of these isosurfaces.

### Density of state (DOS)

The density of state analysis was performed at DFT/B3LYP/6-311G\*\* level of theory to investigate the all-possible states that exist within the specific energy range. Density of states (DOS) analysis is the best method for analyzing fragment interactions and quantifying their effects on the compound's molecular orbital (MO) energy level. DOS analysis determines which fragment interactions most affect MOs energy level. The (DOS) spectra of the drug reveal details on the nature of the interactions happening within the molecule. Positive and negative energy values on the DOS graph shown in (Fig. 11) represent bonding and antibonding orbitals, respectively, in charge distribution around the donor and acceptor moieties. When the value is zero, whether positive or negative, it means that the bonding orbitals do not interact with one another. All the DFT analysis data can be found in (Supporting Table S5).

**Table 5** Quantum chemical descriptors, including local and global parameters, as well as the HOMO–LUMO energy gap (Eg), were theoretically estimated for all of the tailored compounds

Compound	HOMO	LUMO	Eg	$\eta$	$\mu$	S	$\chi$	$\omega$	I	A
	-5.679	-2.441	3.238	1.619	4.060	0.617	-4.060	4.121	2.441	5.679
<b>BENZ-0143</b>										
	-5.563	-1.823	3.740	1.870	3.693	0.534	-3.693	4.132	1.823	5.563
<b>BENZ-0332</b>										
	-5.728	-2.052	3.676	1.838	3.890	0.544	-3.890	4.139	2.052	5.728
<b>BENZ-1070</b>										
	-5.690	-1.811	3.870	1.939	3.750	0.515	-3.750	4.133	1.811	5.690
<b>BENZ-0335</b>										
	-5.612	-1.872	3.740	1.870	3.742	0.534	-3.742	4.000	1.872	5.612
<b>BENZ-0454</b>										
	-5.664	-2.365	3.299	1.649	4.014	0.606	-4.014	4.142	2.365	5.664
<b>BENZ-1292</b>										

These parameters include HOMO–LUMO energy gap (Eg), global hardness ( $\eta$ ), chemical potential ( $\mu$ ), softness (S), electrophilicity index ( $\omega$ ), and electronegativity (X) at the same level of theory as DFT/B3LP/6-311G\*\*

## Molecular dynamics simulations analysis

200 ns MD simulations were carried out to visualize the stability of protein–ligand complexes. The effect of BENZ-0454 and STD on target protein's stability and vice versa is depicted in (Fig. 12A). Protein RMSD remains steady till 55 ns and then steadily increases till  $3.2 \pm 0.05$  Å because of loop/coil region while ligand RMSD depicts a larger peak at 40 ns while remaining inside the active side of the target protein with  $3.2 \pm 0.10$  Å. (Fig. 12B) protein RMSD of STD complex lies within 1.6–3.0 Å with a slight upsurge at 140 ns while global changes in ligand RMSD is higher as compared to BENZ-0454 in contact with 4HJO due to 10 rotatable bonds while remaining stable inside 3.0– $5.6 \pm 0.08$  Å. RMSD values depicted the stability of both complexes.

Local changes in both systems visualize by analyzing RMSF plots (Fig. 13). Atom wise RMSF of BENZ-0454 lies within 2.00 Å while ligand RMSF of STD contains higher

peaks and lies within 3.00 Å as BENZ-0454 has 3 rotatable bonds while STD contains 10 rotatable bonds (Fig. 13A1) and (Fig. 13B1). Residue wise RMSF of BENZ-0454 was less than  $3.2 \pm 0.08$  Å with two higher fluctuations while STD maintain an average RMSF of less than 3.0 Å excluding one higher peak near 150–180 residues that goes beyond 5.4 Å (Fig. 13A2) and (Fig. 13B2). Residue-wise higher RMSF values depict flexibility which indicates the presence of loop/coil regions. Protein secondary structure elements (SSE) visualize during the course of the simulation (Fig. 14). The top plot demonstrates protein SSEs of BENZ-0454 and STD during simulation while the bottom plot shows SSE assignment (alpha-helices with orange color while beta-strands with cyan) of each residue with time. According to the SSE plot, there are 28.94% alpha-helices and 14.77% beta-strands, and a total of 43.71% (Supporting Figure S2).

Figure 15 illustrates the histogram and protein–ligand interaction diagram for both BENZ-0454 and STD



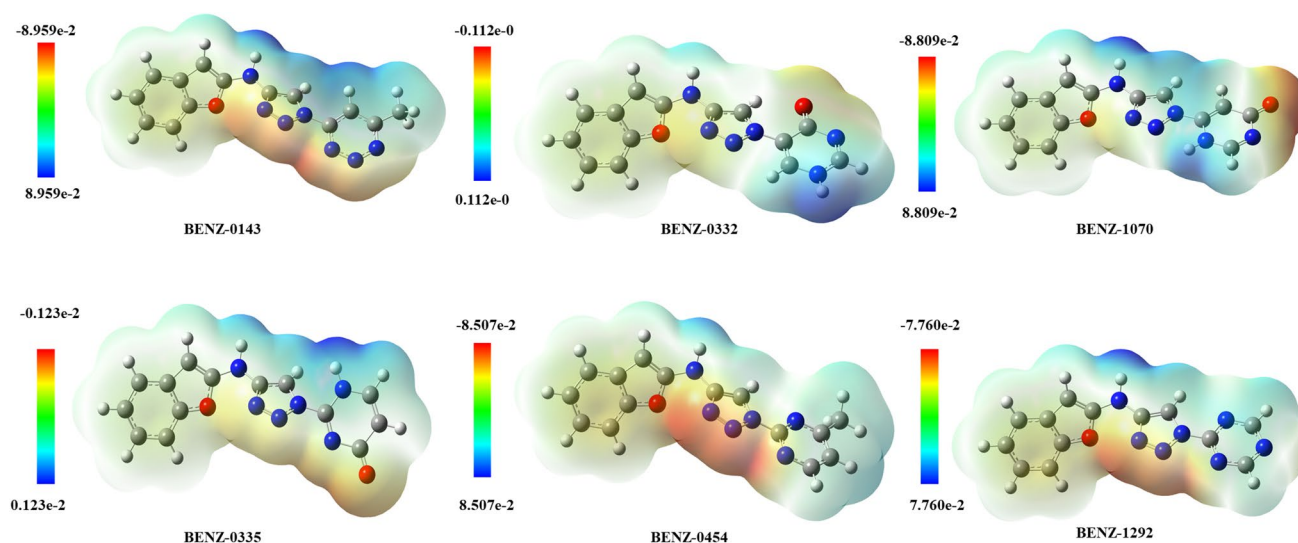


**Fig. 10** MEP maps depicts the electrophilic and nucleophilic attacking sites of best six benzofuran-1,2,3-triazole hybrids. The MEP maps are color-coded, with blue indicating favorable locations for the

nucleophilic attack, red representing hostile regions for the electrophilic attack, and green indicating zero potential sites in the benzofuran-1,2,3-triazole hybrids

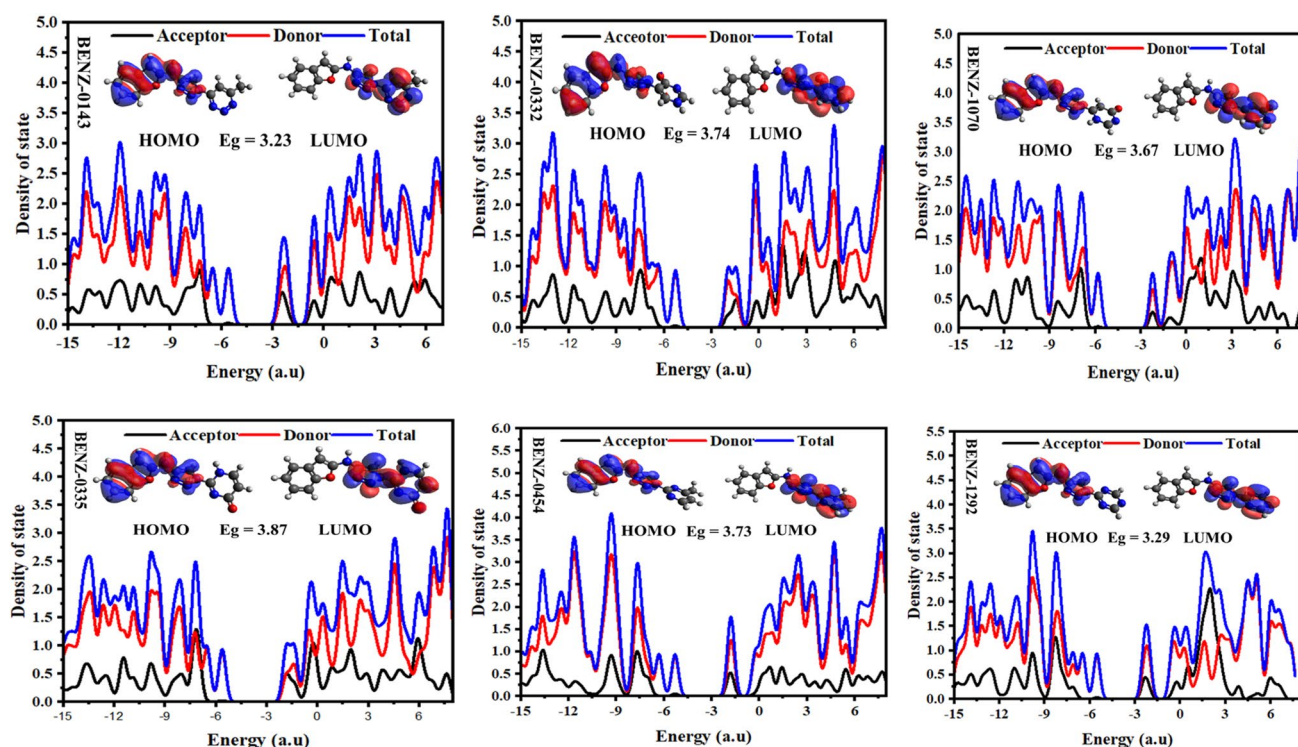


**Fig. 11** Representation of the density of states analysis for the benzofuran-1,2,3-triazole hybrids and their contribution in each fragment is shown

systems. The stacked bar chart for the BENZ-0454 system reveals the majority of water bridges and hydrogen bonds with polar Thr766, Thr830, positively charged (Arg817), and negatively charged conserved (Asp831)

residues. Positively charged Lys721, nonpolar aliphatic Leu820, and aromatic Phe832 make hydrophobic interactions (Fig. 15A). STD bar chart depicts water bridges and hydrogen bond interactions with polar Thr766, Thr830

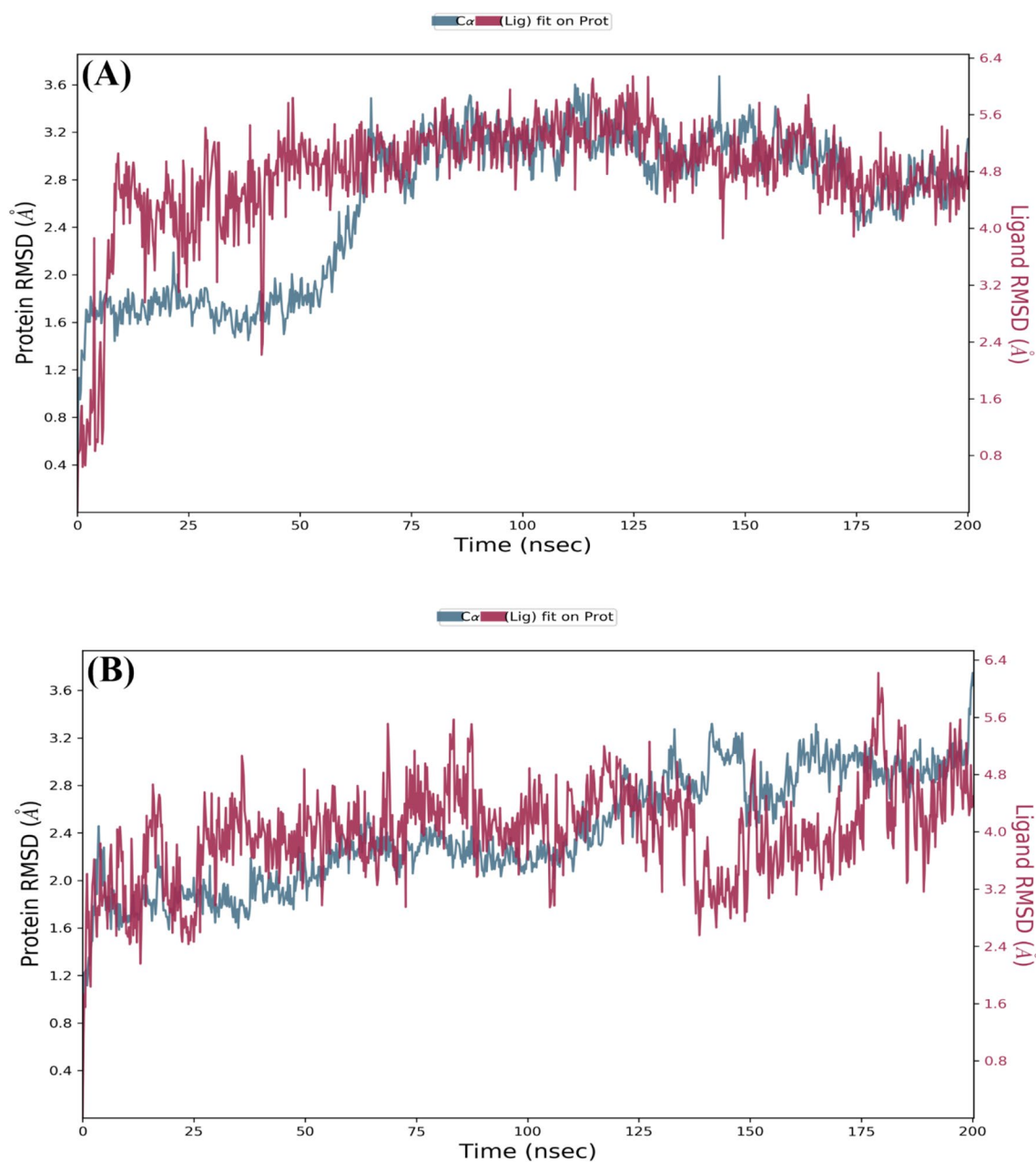


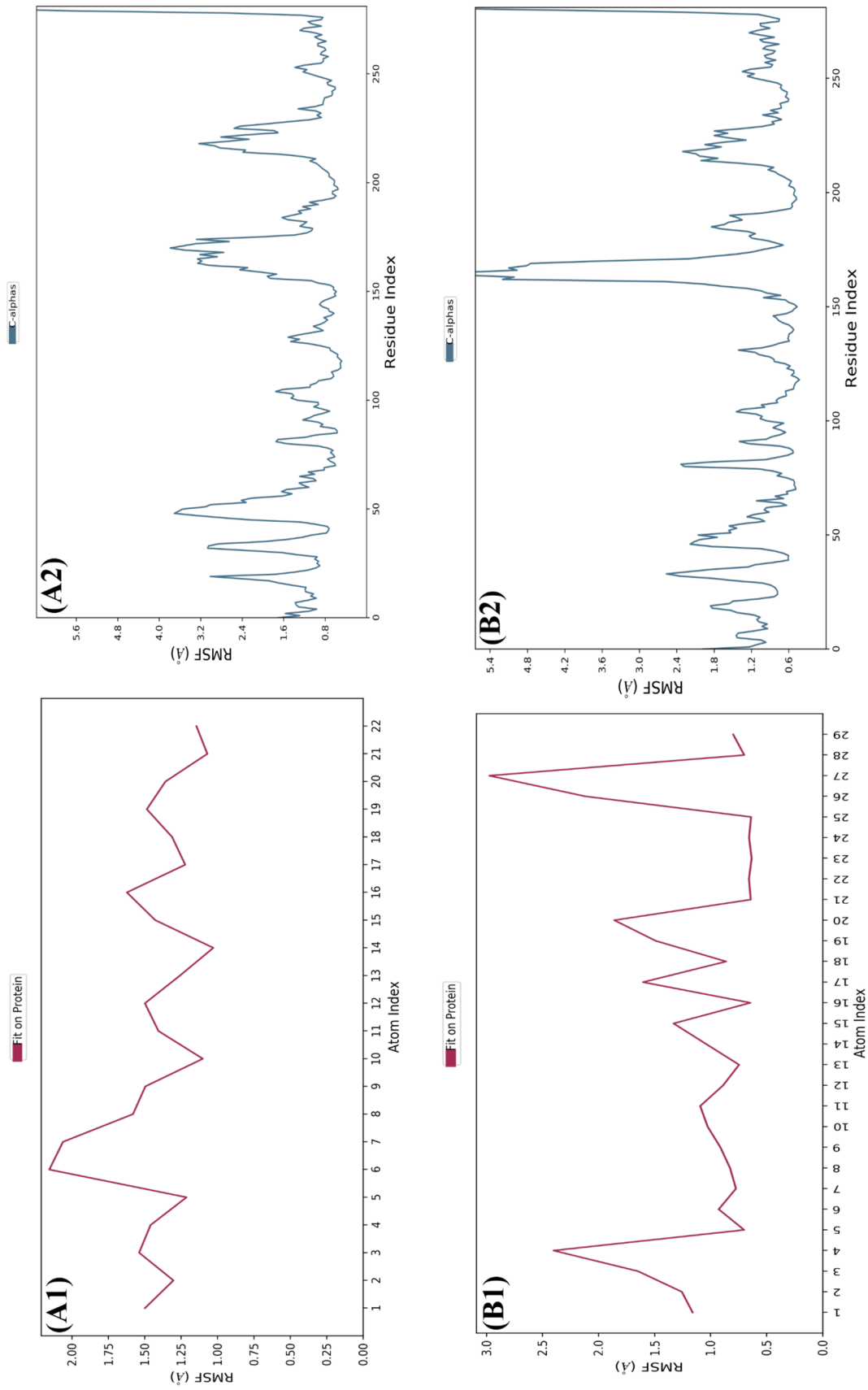
**Fig. 12** (A) RMSD of the C $\alpha$  atoms of EGFR and the best selected ligand BENZ-0454 with time (B) RMSD of EGFR with reference compound overtime. In both images, the left Y-axis showing varia-

tion of protein RMSD (blue line represents results) while right Y-axis show ligand variation (red lines) throughout the simulation

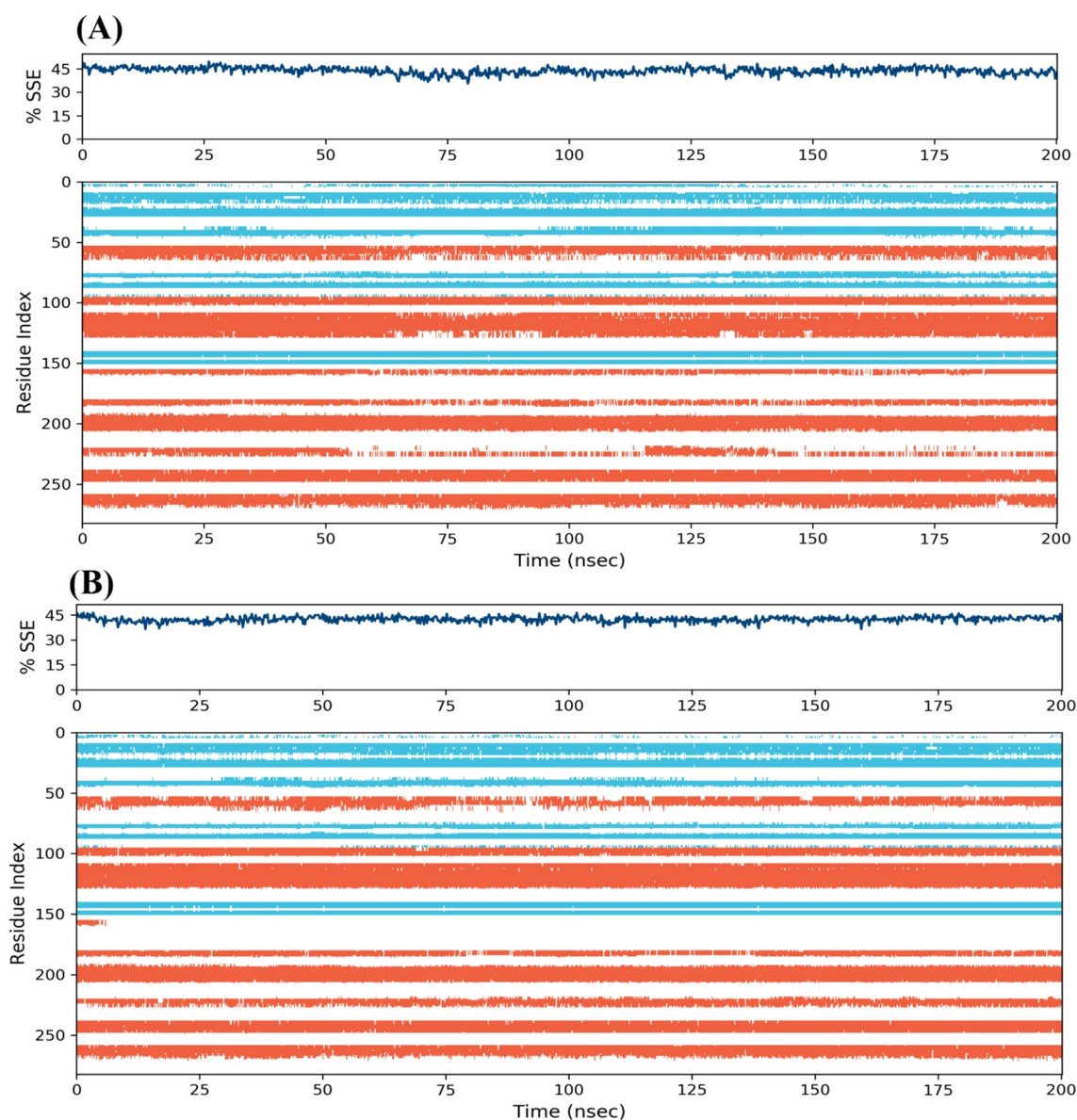
(water bridges with N7 for 77% of the simulation time), Cys773, nonpolar aliphatic Met769 (interact with N6 of STD for 55% of simulation time), Asp776, positively charged Arg817, and negatively charged Asp831 (close range water bridge for 82% of simulation) while nonpolar aliphatic Ala719, Val702, Leu694, Leu820 make hydrophobic interactions (Fig. 15B).

Figure 16 demonstrate a sequential illustration of interactions that BENZ-0454 and STD complexes made

throughout the simulation respectively. The complete list of protein–ligand contacts was shown in the upper panel (blue color), the individual residues that interact with STD and BENZ-0454 were shown in the lower panel (orange color and the residues that make more than one contact with ligand shown in deep orange color). The presence of deep orange bands around Asp831, Thr830, Cys751, Leu820, Leu694, Val702, Lys721, Met742, Leu753, Leu764, Ala719, Thr766, Met769, Cys773, and Asp776 reveals significant



**Fig. 13** (A1) Atom-wise RMSF of BENZ-0454 with respect to target protein EGFR (B1) RMSF of reference molecule with respect to target protein (red colour) while (A2) and (B2) shows Residue-wise RMSF of protein in contact with BENZ-0454 (upper panel) and reference molecule (lower panel)



**Fig. 14** The top plot encapsulates SSE composition during simulation while the bottom plot displays each residue of EGFR receptor (PDB ID: 4HJO and its SSE assignment over time with BENZ-0454 (A) and reference molecule (B)

interactions between these residues and BENZ-0454 and STD compounds. Timelines support the findings of the histogram (Fig. 15).

Figure 17 exhibited ligand torsion profile of BENZ-0454 and STD across the course of 100 ns simulation. The upper panel demonstrates a 2D schematic of both ligands and rotatable bonds represented with different colors while the lower panel depicts a dial (conformation of torsion) and stacked bar charts (potential density of rotatable bonds) which provide information about ligand's conformation in the receptor-bound state. (Fig. 17A) depicts 3 rotatable bonds of BENZ-0454 near  $-90^\circ$ ,  $180^\circ$ ,  $-180^\circ$  while three near  $1.00^\circ$  and a total of 3 rotatable bonds. STD makes 10 rotatable

bonds, 5 near  $180^\circ$ , 3 near  $-90^\circ$  and 2 are in between  $-90^\circ$  to  $90^\circ$  (Fig. 17B). Table 6 represents ligand properties of BENZ-0454 and STD such as RMSD for both systems ranging from 0.6–1.8 Å. rGyr for BENZ-0454 ranging from 4.2–4.6 Å and equilibrated near 4.2 Å. rGyr for STD are in between 4.6–5.0 Å and accomplished equilibrium at 4.9 Å. BENZ-0454's molecular surface area (MoISA) varies from 279 Å<sup>2</sup> to 285 Å<sup>2</sup> while for STD it varies from 380–410 Å<sup>2</sup>. SASA of lead compound and STD-4HJO complex stabilize between 25–75 Å<sup>2</sup> and 50–200 Å<sup>2</sup> respectively. The polar surface area (PSA) for both systems lies within 104–128 Å<sup>2</sup> and 60–90 Å<sup>2</sup> ranges while equilibrated near 125 and 75 Å<sup>2</sup> (Supporting Figure S3).

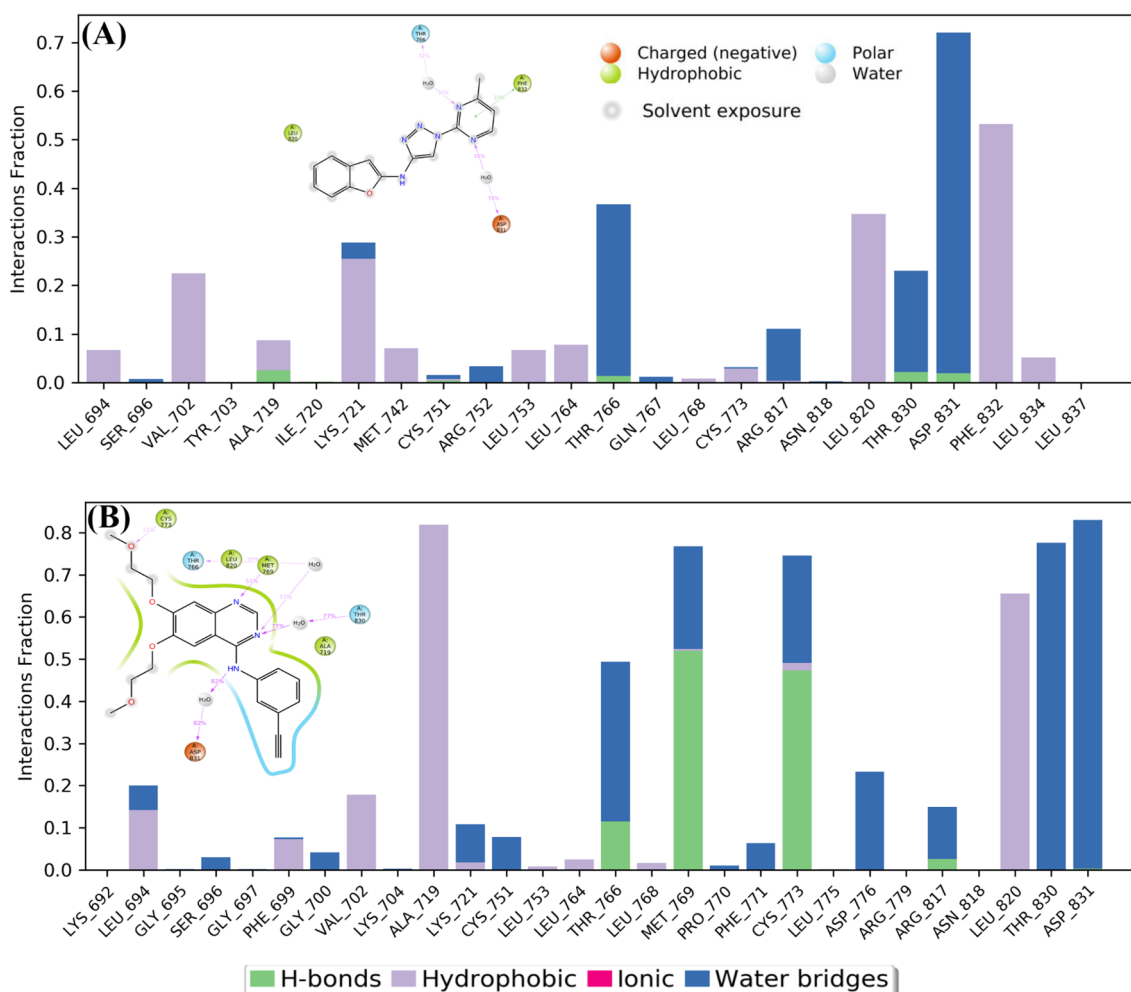


**Fig. 15** (A) Histogram represent summary of all contacts between EGFR and BENZ-0454 while (B) shows interaction information of reference molecule and receptor during MD simulation. As well

as represented protein–ligand interaction for both systems which occur >30.0% of simulation time

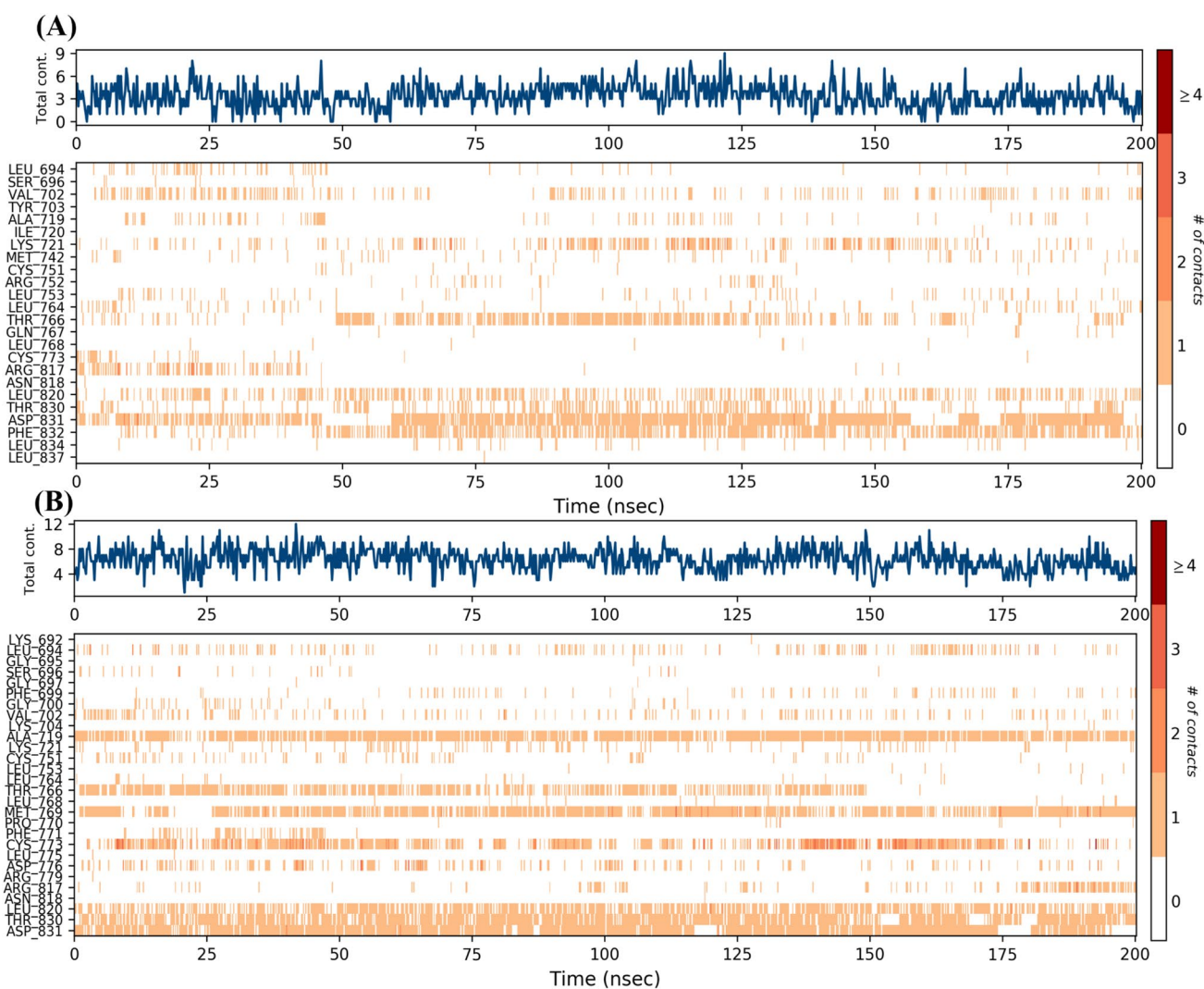
## Binding free energy calculations

In order to calculate the binding free energies of both complexes more quickly, MMGBSA analysis was used (Fig. 18). These computed energy profiles provide comprehensive molecular indications that could be very helpful for the design and development of a drug. MMGBSA is a widely used, highly dynamic, and cost-effective computational technique as it computes coulombic (−6.4415, −18.7182 kcal/mol), covalent (3.034, 8.4807 kcal/mol), lipophilic (−12.6161, −20.7386 kcal/mol), van der Waals (−48.8510, −54.3601 kcal/mol), strain energy (2.2893, 8.3226 kcal/mol), hydrogen bonding (−2.3107, −1.2375 kcal/mol) and the total binding free energy is −45.6046, −59.3587 kcal/mol for BENZ-0454 and STD complexes. Van der Waals contributes more than others

and total binding energies (negative values) depict the interaction of ligands that point out inhibition phenomena. The total binding free energy ( $\Delta G_{\text{bind}}$ ) supports BENZ-0454 to inhibit the EGFR protein.

## Discussion

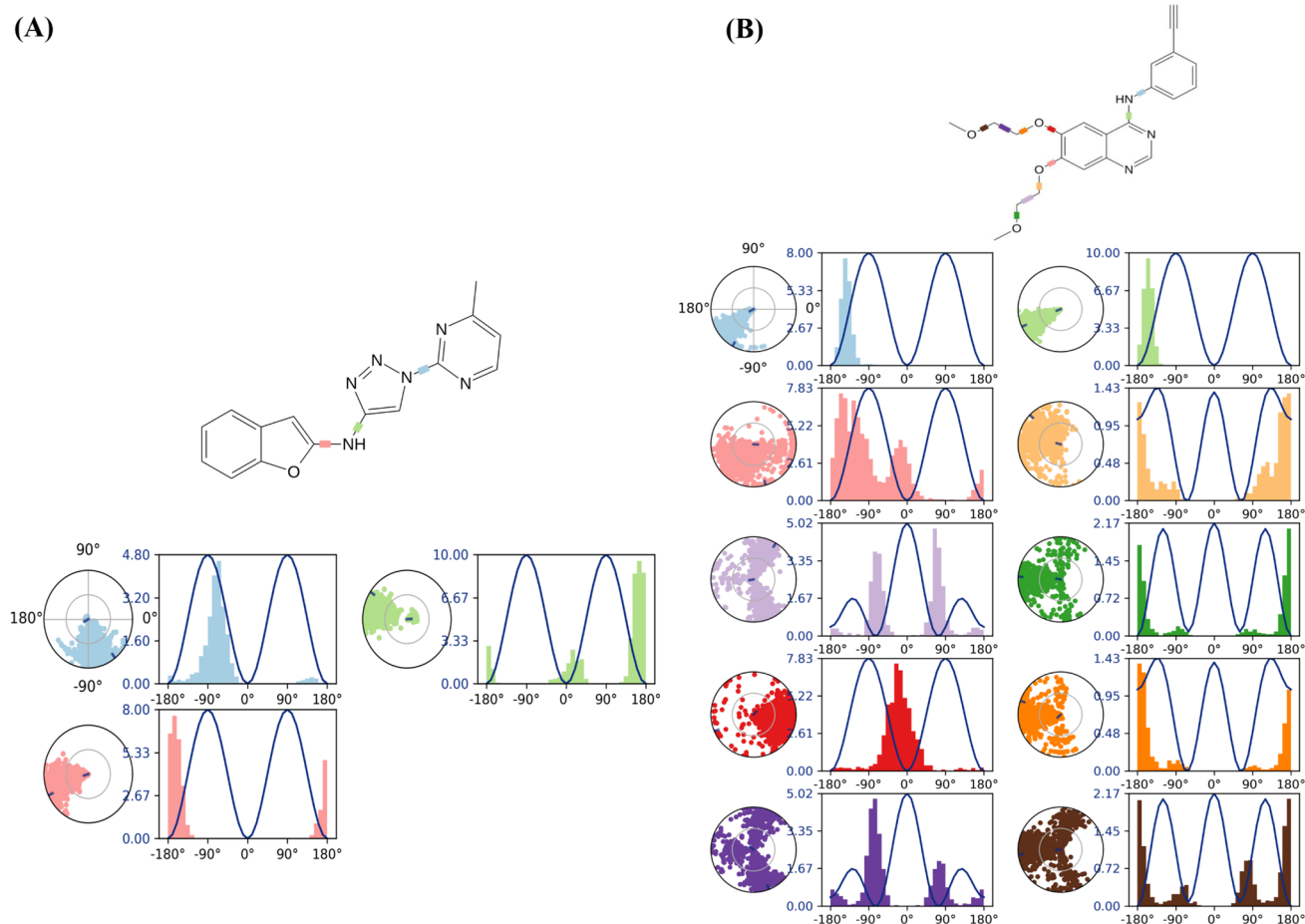
Triazole-based compounds are a promising new class of therapeutic agents for the treatment of lung cancer. These compounds have been shown to be potent and selective inhibitors of the epidermal growth factor receptor (EGFR), which is a key driver of lung cancer growth. Yan et al. conducted a study where they designed and synthesized a novel series of dianilinopyrimidines as inhibitors of EGFR. The target compounds were characterized using



**Fig. 16** The top plot encapsulates SSE composition during simulation while the bottom plot displays each residue of anticancer target EGFR (PDB ID: 4HJO and its SSE assignment over time with BENZ-0454 (A) and reference molecule (B)

$^1\text{H-NMR}$ ,  $^{13}\text{C-NMR}$ , and HRMS analyses. Subsequently, the researchers evaluated the inhibitory effects of these compounds against EGFR and tumor cells including A549, PC-3, and HepG2. The results revealed that certain compounds exhibited promising anti-tumor activities. Notably demonstrated the highest activity against all tumor cells, with  $\text{IC}_{50}$  values of  $0.56\ \mu\text{M}$ ,  $2.46\ \mu\text{M}$ , and  $2.21\ \mu\text{M}$ , respectively. Further investigations demonstrated that the compounds induced apoptosis in A549 cells and arrested A549 cells in the G2/M phase (Yan et al. 2022). Chaube, Udit J., et al. investigated the binding interactions of AZD-2014 with the mTOR protein in order to identify crucial interactions necessary for designing potent mTOR inhibitors. This was complemented by QSAR studies. Virtual screening studies using pharmacophore-based approaches identified a core scaffold, namely THQ (Tetrahydro-Quinoline derivatives). Subsequently, 31 THQ

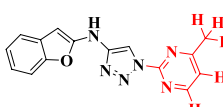
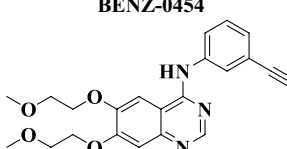
derivatives were synthesized and characterized based on molecular docking interactions. The compounds were then subjected to cellular mTOR enzyme assay and evaluated for their antiproliferative activity against a panel of cancerous cell lines (Chaube et al. 2021). Zhou, Wenjun, et al. designed and synthesized a series of covalent inhibitors targeting EGFR-T790M using purine as the base structure. These inhibitors were then assessed for their antiproliferative effects in cellular assays using various cancer cell lines. Remarkably, certain compounds demonstrated the ability to effectively block the proliferation of EGFR-T790M PC9 cells, with  $\text{EC}_{50}$  values falling within the low nanomolar range (Zhou et al. 2011). Triazole-based compounds have also been shown to be effective in inhibiting the growth of EGFR-expressing lung cancer cells in-vitro and in-vivo (Gariganti et al. 2023). One of the most well-known triazole-based compounds is gefitinib,



**Fig. 17** (A) Torsions plot of BENZ-0454 represent conformational evolution of ligand's rotatable bonds throughout the simulation. (B) ligand torsion plot with reference molecule. The top panel represent

2d schematic of BENZ-0454 and reference molecule while bottom panel shows dial plot and bar plots. The values of the potential are on the left Y-axis of the chart represented in kcal/mol

**Table 6** BENZ-0454 and reference ligand (Erlotinib) properties determined via MD simulation i.e., Intramolecular Hydrogen Bonds (intraHB), RMSD, Molecular Surface Area (MolSA), Radius of Gyration (rGyr), Polar Surface Area (PSA), Solvent Accessible Surface Area (SASA)

Ligand properties	RMSD	rGyr	intraHB	MolSA	SASA	PSA
 <b>BENZ-0454</b>	1.8	4.6	0	285	75	128
 <b>Reference molecule</b>	1.8	5.0	0	410	200	90

which was approved by the FDA for the treatment of lung cancer (Cohen et al. 2004). Gefitinib is a potent and selective inhibitor of EGFR, and it has been shown to be effective in patients with EGFR-mutant lung cancer (Yano et al. 2003). Other triazole-based compounds that

are currently in clinical development for the treatment of lung cancer include osimertinib, afatinib, and rociletinib. The compounds have shown promise in clinical trials, and they could represent new standard-of-care treatments for lung cancer in the future (Singh and Jadhav 2018). The

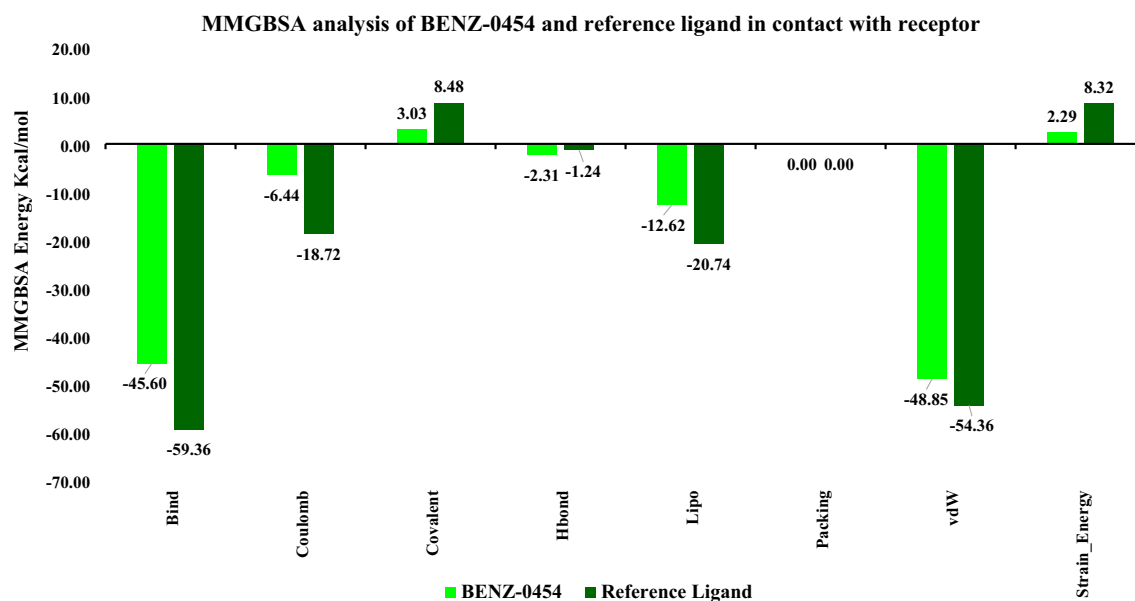


**Fig. 18** MM-GBSA analysis of BENZ-0454 and reference ligand EGFR Protein (PDB ID: 4HJO) with different energies i.e. Binding free energy, Coulombic, Covalent, Hydrogen binding energy, Lipo-

philic, Generalized Born electrostatic solvation energy and Van der Waals binding energy

development of triazole-based compounds as therapeutic agents for lung cancer is an exciting and rapidly advancing field. As our knowledge of the molecular intricacies underlying lung cancer deepens, we can anticipate the emergence of even more potent and selective triazole-based compounds in the future. Ongoing research endeavors are dedicated to enhancing the therapeutic efficacy of these compounds and addressing resistance mechanisms associated with EGFR inhibition (Russo et al. 2015). Through strategies like structure–activity relationship studies, molecular modeling, and rational drug design, with the aim to discover novel triazole-based compounds with improved pharmacological properties (Zubair and Bandyopadhyay 2023). These advancements hold immense potential in expanding the range of targeted therapies available and ultimately improving outcomes for patients with lung cancer. Continued exploration and innovation in this area will undoubtedly shape the future of lung cancer treatment.

## Conclusion

The outcomes of the study indicate that the designed benzofuran-1,2,3-triazole hybrids display a promising interaction with EGFR, thus holding potential as therapeutic agents for lung cancer treatment. The molecular docking and dynamics simulations revealed that the designed molecules bind effectively to the active site of EGFR and have stable interactions. The in-silico ADME and toxicity studies indicated that the

designed compounds have good drug-likeness properties and low toxicity potential. The DFT studies provided valuable insights into the electronic properties of the selected best ligands, which could play a crucial role in their biological activity. In conclusion, this study provides useful insights into the design and development of novel EGFR inhibitors for lung cancer treatment, and the results of this study could serve as a foundation for further experimental studies. The findings of this study demonstrate the potential of benzofuran-1,2,3-triazole hybrids as a new class of EGFR inhibitors with therapeutic potential for the treatment of lung cancer. To fully explore the therapeutic potential of the recently discovered benzofuran-1,2,3-triazole hybrids BENZ-0454, BENZ-0143, BENZ-1292, BENZ-0335, BENZ-0332, and BENZ-1070 as treatments for human lung cancer, several critical steps must be taken in the future. These compounds must be synthesized in adequate quantities to enable extensive testing and further research. Moreover, there is a need to explore and develop more efficient and optimized methods of synthesis to improve the potency and efficacy of these compounds. The effectiveness of these compounds against EGFR mutations must be established through thorough in-vitro and in-vivo experiments. It is essential to test these compounds on several cancer cell types and animal models to ensure their effectiveness on different types of cancer. Finally, detailed in-vitro and in-vivo experiments must be conducted to investigate the potential of these compounds to target human lung cancer. The mechanisms of action and therapeutic potential of BENZ-0454, BENZ-0143, BENZ-1292, BENZ-0335, BENZ-0332, and BENZ-1070 must be



studied in-depth to fully understand their potential as lung cancer treatments. The results of this study furnish valuable insights into the design and development of novel EGFR inhibitors for the treatment of lung cancer, and these findings could be the basis for further experimental studies.

**Supplementary Information** The online version contains supplementary material available at <https://doi.org/10.1007/s40203-023-00157-1>.

**Acknowledgements** The authors express their gratitude to the Department of Pharmaceutical Chemistry, School of Pharmaceutical Sciences, Shoolini University, Solan, Himachal Pradesh-173229, India for the support.

**Author contributions** SK: investigation, writing-original draft, methodology, designed and conceived the study. IA: MD simulations and MM-GBSA analysis. FA and NK: Density-functional theory analysis. MKG and MG: Conceptualization. SK: review & editing. DK: Supervision, methodology, and project administration. All authors have read and agreed to the published version of the manuscript.

**Funding** The authors received no financial support for the research, authorship, and publication of this article.

**Data availability** Data will be made available on request.

## Declarations

**Conflict of interest** The authors confirm that there are no known conflicts of interest associated with this publication and no significant financial support for this work that could have influenced its outcome.

## References

- Abbas F, Ali U, Ahmad HMR, Tallat A, Shehzad A, Zeb Z et al (2022a) Body centered non-fullerene acceptors substitution on triangular shaped Sub-phthalocyanines (SubPcs) based A-D-A organic solar cells: a step toward new strategies for better performances. *Opt Quantum Electron* 54:1–15. <https://doi.org/10.1007/s11082-021-03413-w>
- Abbas F, Ali U, Muhammad Rizwan Ahmad H, Tallat A, Shehzad A, Zeb Z et al (2022b) Role of Iodo-Substituted Subphthalocyanine (Subpcs)  $\pi$ -conjugated aromatic N-fused di-Iminoisonidole units on the performance of non-fullerene small organic solar cells. *Comput Theor Chem*. 1207:113508. <https://doi.org/10.1016/J.COMPTC.2021.113508>
- Boch C, Kollmeier J, Roth A, Stephan-Falkenau S, Misch D, Grüning W et al (2013) The frequency of EGFR and KRAS mutations in non-small cell lung cancer (NSCLC): routine screening data for central Europe from a cohort study. *BMJ Open* 3:e002560. <https://doi.org/10.1136/BMJOPEN-2013-002560>
- Chaube UJ, Rawal R, Jha AB, Variya B, Bhatt HG (2021) Design and development of Tetrahydro-Quinoline derivatives as dual mTOR-C1/C2 inhibitors for the treatment of lung cancer. *Bioorg Chem* 106:104501. <https://doi.org/10.1016/j.bioorg.2020.104501>
- Chaudhari R, PyMine LZ (2015) A PyMOL plugin to integrate and visualize data for drug discovery bioinformatics. *BMC Res Notes* 8(1):1–5. <https://doi.org/10.1186/s13104-015-1483-3>
- Cheng WC, Shen YC, Chien CR, Liao WC, Chen CH, Hsia TC et al (2022) The optimal therapy strategy for epidermal growth factor receptor-mutated non-small cell lung cancer patients with brain metastasis: a real-world study from Taiwan. *Thorac Cancer* 13(10):1505–1512. <https://doi.org/10.1111/1759-7714.14423>
- Cohen MH, Williams GA, Sridhara R, Chen G, McGuinn WD, Morse D et al (2004) United States food and drug administration drug approval Summary Gefitinib (ZD1839; Iressa) tablets. *Clin Cancer Res* 10(4):1212–1218. <https://doi.org/10.1158/1078-0432.ccr-03-0564>
- Cooper ZD (2016) Adverse effects of synthetic cannabinoids: management of acute toxicity and withdrawal. *Curr Psychiatry Rep* 18(5):1–10. <https://doi.org/10.1007/2Fs11920-016-0694-1>
- Cosconati S, Forli S, Perryman AL, Harris R, Goodsell DS, Olson AJ. (2010) Virtual screening with AutoDock: theory and practice 5(6):597–607. <https://doi.org/10.1517/17460441.2010.484460>
- Daina A, Michielin O, Zoete V (2017) SwissADME: a free web tool to evaluate pharmacokinetics, drug-likeness and medicinal chemistry friendliness of small molecules. *Sci Rep* 7(1):1–13. <https://doi.org/10.1038/srep42717>
- Dallakyan S, Olson AJ (2015) Small-molecule library screening by docking with PyRx. *Methods Mol Biol* 1263:243–250. [https://doi.org/10.1007/978-1-4939-2269-7\\_19](https://doi.org/10.1007/978-1-4939-2269-7_19)
- Danielson ML, Hu B, Shen J, Desai P (2017) In silico ADME techniques used in early-phase drug discovery. *AAPS Adv Pharmac Sci Ser* 25:81–117. [https://doi.org/10.1007/978-3-319-50042-3\\_4](https://doi.org/10.1007/978-3-319-50042-3_4)
- Daoud NE-H, Borah P, Deb PK, Venugopala KN, Hourani W, Alzweiri M et al (2021) ADMET profiling in drug discovery and development: perspectives of in silico, in vitro and integrated approaches. *Curr Drug Metab* 22(7):503–522. <https://doi.org/10.2174/1389200222666210705122913>
- Darvish Ganji M, Mirzaei S, Dalirandeh Z (2017) Molecular origin of drug release by water boiling inside carbon nanotubes from reactive molecular dynamics simulation and DFT perspectives. *Sci Rep* 7(1):1–13. <https://doi.org/10.1038/s41598-017-04981-2>
- Dearden JC (2003) In silico prediction of drug toxicity. *J Comput Aided Mol Des* 2–4:119–127. <https://doi.org/10.1023/A:1025361621494>
- Frisch MJ, Trucks GW, Schlegel HB, Scuseria GE, Robb MA, Cheeseman JR et al (2016) Gaussian 16. Gaussian, Inc. Wallingford, CT. <https://gaussian.com/gaussian16/>
- Gariganti N, Loke SK, Pagadala E, Chinta P, Poola B, Chetti P et al (2023) Design, synthesis, anticancer activity of new amide derivatives derived from 1,2,3-triazole-benzofuran hybrids: an insights from molecular docking, molecular dynamics simulation and DFT studies. *J Mol Struct* 1273:134250. <https://doi.org/10.1016/J.MOLSTRUC.2022.134250>
- Genheden S, Ryde U (2015) The MM/PBSA and MM/GBSA methods to estimate ligand-binding affinities. *Expert Opin Drug Discov* 10(5):449–461. <https://doi.org/10.1517/2F17460441.2015.1032936>
- Gill PMW, Johnson BG, Pople JA, Frisch MJ (1992) The performance of the Becke—Lee—Yang—Parr (B—LYP) density functional theory with various basis sets. *Chem Phys Lett* 197(4–5):499–505
- Hofman P, Mani SA, Calin GA, Wistuba II, Bianchi F, Riudavets M et al (2022) Radon and lung cancer: current trends and future perspectives. *Cancers* 14(13):3142. <https://doi.org/10.3390/CANCERS14133142>
- Honorio M, Moda L, Andricopulo D (2013) Pharmacokinetic properties and in silico ADME modeling in drug discovery. *Med Chem* 9(2):163–176. <https://doi.org/10.2174/1573406411309020002>
- Hu Y, Zhou L, Zhu X, Dai D, Bao Y, Qiu Y (2019) Pharmacophore modeling, multiple docking, and molecular dynamics studies on Wee1 kinase inhibitors. *J Biomol Struct Dyn* 37(10):2703–2715. <https://doi.org/10.1080/07391102.2018.1495576>
- Ihn HJ, Lee D, Lee T, Shin HI, Bae YC, Kim SH, et al (2015) The 1,2,3-triazole derivative KP-A021 suppresses osteoclast




- differentiation and function by inhibiting RANKL-mediated MEK-ERK signaling pathway. *240*(12):1690–7. <https://doi.org/10.1177/1535370215576310>
- Jacobson MP, Pincus DL, Rapp CS, Day TJJ, Honig B, Shaw DE et al (2004) A hierarchical approach to all-atom protein loop prediction. *Proteins* 55(2):351–367. <https://doi.org/10.1002/PROT.10613>
- Jia CY, Li JY, Hao GF, Yang GF (2020) A drug-likeness toolbox facilitates ADMET study in drug discovery. *Drug Discov Today* 25(1):248–258. <https://doi.org/10.1016/J.DRUDIS.2019.10.014>
- Kerpel-Fronius A, Tammemägi M, Cavic M, Henschke C, Jiang L, Kazerooni E et al (2022) Screening for lung cancer in individuals who never smoked: an international association for the study of lung cancer early detection and screening committee report. *J Thorac Oncol* 17(1):56–66. <https://doi.org/10.1016/J.JTHO.2021.07.031>
- Kontoyianni M (2017) Docking and virtual screening in drug discovery. *Methods Mol Biol* 1647:255–266. [https://doi.org/10.1007/978-1-4939-7201-2\\_18](https://doi.org/10.1007/978-1-4939-7201-2_18)
- Kumar A, Petri ET, Halmos B, Boggon TJ (2008) The structure and clinical relevance of the EGF receptor in human cancer. *J Clin Oncol* 26(10):1742. <https://doi.org/10.1200/JCO.2007.12.1178>
- Kumar S, Sharma AK, Lalhlenmawia H, Kumar D (2021) Natural compounds targeting major signaling pathways in lung cancer. *Target Cell Signal Pathways Lung Dis*. [https://doi.org/10.1007/978-981-33-6827-9\\_37](https://doi.org/10.1007/978-981-33-6827-9_37)
- Kumar S, Abbas F, Ali I, Gupta MK, Kumar S, Garg M et al (2023) Integrated network pharmacology and in-silico approaches to decipher the pharmacological mechanism of *Selaginella tamariscina* in the treatment of non-small cell lung cancer. *Phytomed plus* 3(2):100419. <https://doi.org/10.1016/J.PHYPLU.2023.100419>
- Kurter H, Mert-Ozupuk N, Ellidokuz H, Calibasi-Kocal G (2022) In-silico drug-likeness analysis, ADME properties, and molecular docking studies of cyanidin-3-arabinoxide, pelargonidin-3-glucoside, and peonidin-3-arabinoxide as natural anticancer compounds against acting receptor-like kinase 5 receptor. *Anticancer Drugs* 33(6):517–522. <https://doi.org/10.1097/CAD.0000000000001297>
- Li BH, Ge JQ, Wang YL, Wang LJ, Zhang Q, Bian C (2021) Ligand-based and docking-based virtual screening of MDM2 inhibitors as potent anticancer agents. *Comput Math Methods Med*. <https://doi.org/10.1155/2021/3195957>
- Liang T, Sun X, Li W, Hou G, Gao F (2021) 1,2,3-triazole-containing compounds as anti-lung cancer agents: current developments, mechanisms of action, and structure-activity relationship. *Front Pharmacol* 12:1374
- Martin-Fernandez ML, Clarke DT, Roberts SK, Zanetti-Domingues LC, Gervasio FL (2019) Structure and dynamics of the EGF receptor as revealed by experiments and simulations and its relevance to non-small cell lung cancer. *Cells*. <https://doi.org/10.3390/cells8040316>
- Mohammadi MD, Abbas F, Louis H, Mathias GE, Unimuke TO (2022) Trapping of CO, CO<sub>2</sub>, H<sub>2</sub>S, NH<sub>3</sub>, NO, NO<sub>2</sub>, and SO<sub>2</sub> by polyoxometalate compound. *Comput Theor Chem* 1215:113826. <https://doi.org/10.1016/J.COMPTC.2022.113826>
- Morris GM, Ruth H, Lindstrom W, Sanner MF, Belew RK, Goodsell DS et al (2009) AutoDock4 and AutoDockTools4: automated docking with selective receptor flexibility. *J Comput Chem* 30(16):2785–2791. <https://doi.org/10.1002/JCC.21256>
- Napiórkowska M, Cieslakcislak M, Kazmierczakkazmierczak-Baráńska J, Królewska-Golfńska K, Nawrot B, Cieslak M et al (2019) Synthesis of new derivatives of benzofuran as potential anticancer agents. *Molecules* 24(8):1529. <https://doi.org/10.3390/molecules24081529>
- O'Boyle NM, Banck M, James CA, Morley C, Vandermeersch T, Hutchison GR (2011) Open babel: an open chemical toolbox. *J Cheminform Biomed Central* 3(10):1–14. <https://doi.org/10.1186/1758-2946-3-33>
- Othman EM, Fayed EA, Husseiny EM, Abulkhair HS (2022) Rationale design, synthesis, cytotoxicity evaluation, and in silico mechanistic studies of novel 1,2,3-triazoles with potential anticancer activity. *New J Chem* 46(25):12206–12216. <https://doi.org/10.1039/D2NJ02061K>
- Pandi S, Kulanthaivel L, Subbaraj GK, Rajaram S, Subramanian S (2022) Screening of potential breast cancer inhibitors through molecular docking and molecular dynamics simulation. *Biomed Res Int*. <https://doi.org/10.1155/2022/3338549>
- Panigrahi D, Mishra A, Sahu SK (2020) Pharmacophore modelling, QSAR study, molecular docking and insilico ADME prediction of 1,2,3-triazole and pyrazolopyridones as DprE1 inhibitor antitubercular agents. *SN Appl Sci* 2(5):1–28. <https://doi.org/10.1007/s42452-020-2638-y>
- Park JH, Liu Y, Lemmon MA, Radhakrishnan R (2012) Erlotinib binds both inactive and active conformations of the EGFR tyrosine kinase domain. *Biochem J* 448(3):417–423. <https://doi.org/10.1042/BJ20121513>
- Paul Gleeson M, Hersey A, Hannongbua S (2011) In-silico ADME models: a general assessment of their utility in drug discovery applications. *Curr Top Med Chem* 11(4):358–381. <https://doi.org/10.2174/156802611794480927>
- Pinzi L, Rastelli G (2019) Molecular docking: shifting paradigms in drug discovery. *Int J Mol Sci* 20(18):4331. <https://doi.org/10.3390/IJMS20184331>
- Qi ZY, Hao SY, Tian HZ, Bian HL, Hui L, Chen SW (2020) Synthesis and biological evaluation of 1-(benzofuran-3-yl)-4-(3,4,5-trimethoxyphenyl)-1H-1,2,3-triazole derivatives as tubulin polymerization inhibitors. *Bioorg Chem* 94:103392. <https://doi.org/10.1016/J.BIOORG.2019.103392>
- Raies AB, Bajic VB (2016) In silico toxicology: computational methods for the prediction of chemical toxicity. *Wiley Interdiscip Rev Comput Mol Sci* 6(2):147–172. <https://doi.org/10.1002/WCMS.1240>
- Rasheed MA, Iqbal MN, Saddick S, Ali I, Khan FS, Kanwal S et al (2021) Identification of lead compounds against scm (Fms10) in enterococcus faecium using computer aided drug designing. *Life* 11(2):77. <https://doi.org/10.3390/life11020077>
- Rodriguez-Canales J, Parra-Cuentas E, Wistuba II (2016) Diagnosis and molecular classification of lung cancer. *Cancer Treat Res* 170:25–46. [https://doi.org/10.1007/978-3-319-40389-2\\_2](https://doi.org/10.1007/978-3-319-40389-2_2)
- Russo A, Franchina T, Ricciardi GRR, Picone A, Ferraro G, Mariangela Z et al (2015) A decade of EGFR inhibition in EGFR-mutated non small cell lung cancer (NSCLC): Old successes and future perspectives. *Oncotarget* 6(29):26814. <https://doi.org/10.18632/oncotarget.4254>
- Sahoo R, Babu VC, Patil Okaly G, Rao S, Nargund A et al (2011) Screening for EGFR mutations in lung cancer, a report from India. *Lung Cancer* 73(3):316–319. <https://doi.org/10.1016/J.LUNGCAN.2011.01.004>
- Sander T, Freyss J, von Korff M, Reich JR, Rufener C (2009) OSIRIS, an entirely in-house developed drug discovery informatics system. *J Chem Inf Model* 49(2):232–246. <https://doi.org/10.1021/ci800305f>
- Sharma R (2022) Mapping of global, regional and national incidence, mortality and mortality-to-incidence ratio of lung cancer in 2020 and 2050. *Int J Clin Oncol* 27(4):665–675. <https://doi.org/10.1007/S10147-021-02108-2>
- Sharma A, Shambhwani D, Pandey S, Singh J, Lalhlenmawia H, Kumarasamy M et al (2022) Advances in lung cancer treatment using nanomedicines. *ACS Omega* 8(1):10–41. <https://doi.org/10.1021/acsomega.2c04078>
- Shaw Research DE. Desmond. <https://www.deshawresearch.com/resources.html> (accessed 21 Jan 2023)

- Sigismund S, Avanzato D, Lanzetti L (2018) Emerging functions of the EGFR in cancer. *Mol Oncol* 12(1):3–20. <https://doi.org/10.1002/1878-0261.12155>
- Singh M, Jadhav HR (2018) Targeting non-small cell lung cancer with small-molecule EGFR tyrosine kinase inhibitors. *Drug Discov Today* 23(3):745–753. <https://doi.org/10.1016/j.drudis.2017.10.004>
- Stanzione F, Giangreco I, Cole JC (2021) Use of molecular docking computational tools in drug discovery. *Prog Med Chem* 60:273–343. <https://doi.org/10.1016/BS.PMCH.2021.01.004>
- Terstappen GC, Reggiani A (2001) In silico research in drug discovery. *Trends Pharmacol Sci Elsevier Curr Trends* 22(1):23–26. [https://doi.org/10.1016/S0165-6147\(00\)01584-4](https://doi.org/10.1016/S0165-6147(00)01584-4)
- Thandra KC, Barsouk A, Saginala K, Aluru JS, Barsouk A (2021) Epidemiology of lung cancer. *Contemp Oncol* 25(1):45–52. <https://doi.org/10.5114/WO.2021.103829>
- Tian S, Wang J, Li Y, Li D, Xu L, Hou T (2015) The application of in silico drug-likeness predictions in pharmaceutical research. *Adv Drug Deliv Rev* 86:2–10. <https://doi.org/10.1016/J.ADDR.2015.01.009>
- Upadhyay J, Gajjar A, Suhagia BN (2019) Combined ligand-based and structure-based virtual screening approach for identification of new dipeptidyl peptidase 4 inhibitors. *Curr Drug Discov Technol* 16(4):426–436. <https://doi.org/10.2174/157016381566618092611558>
- Vaccarella S, Georges D, Bray F, Ginsburg O, Charvat H, Martikainen P et al (2022) Socioeconomic inequalities in cancer mortality between and within countries in Europe: a population-based study. *Lancet Regional Health* 28:100551. <https://doi.org/10.1016/J.LANEPE.2022.100551>
- Valerio LG (2009) In silico toxicology for the pharmaceutical sciences. *Toxicol Appl Pharmacol* 241(3):356–370. <https://doi.org/10.1016/J.TAAP.2009.08.022>
- Van Assche K, Ferdinande L, Lievens Y, Vandecasteele K, Surmont V (2014) EGFR mutation positive stage IV non-small-cell lung cancer: treatment beyond progression. *Front Oncol* 4:350. <https://doi.org/10.3389/FONC.2014.00350>
- VLife Sciences M. Vlife MDS. <https://www.vlifesciences.com/products/VLifeMDS/Molsign.php> (accessed 20 Jan 2023).
- Wang Y, Xing J, Xu Y, Zhou N, Peng J, Xiong Z et al (2015) In silico ADME/T modelling for rational drug design. *Q Rev Biophys* 48(4):488–515. <https://doi.org/10.1017/S0033583515000190>
- Xiong G, Wu Z, Yi J, Fu L, Yang Z, Hsieh C et al (2021) ADMETlab 2.0: an integrated online platform for accurate and comprehensive predictions of ADMET properties. *Nucleic Acids Res* 49(1):5–14. <https://doi.org/10.1093/nar/gkab255>
- Yan L, Wang Q, Liu L, Le Y (2022) Design, synthesis and biological evaluation of a series of dianilino-pyrimidines as EGFR inhibitors. *J Enzyme Inhib Med Chem* 37(1):832–843. <https://doi.org/10.1080/14756366.2022.2046567>
- Yano S, Yamaguchi M, Dong RP (2003) EGFR tyrosine kinase inhibitor “gefitinib (Iressa)” for cancer therapy. *Nihon Yakurigaku Zasshi* 122(6):491–497. <https://doi.org/10.1254/fpj.122.491>
- Yarden Y (2001) The EGFR family and its ligands in human cancer: signalling mechanisms and therapeutic opportunities. *Eur J Cancer* 37:3–8. [https://doi.org/10.1016/S0959-8049\(01\)00230-1](https://doi.org/10.1016/S0959-8049(01)00230-1)
- Zhang X, Perez-Sanchez H, Lightstone FC (2017) A comprehensive docking and MM/GBSA rescoring study of ligand recognition upon binding antithrombin. *Curr Top Med Chem* 17(14):1631. <https://doi.org/10.2174/1568026616666161117112604>
- Zhong ZH, Yi ZL, Zhao YD, Wang J, Jiang ZB, Xu C et al (2022) Pyronaridine induces apoptosis in non-small cell lung cancer cells by upregulating death receptor 5 expression and inhibiting epidermal growth factor receptor. *Chem Biol Drug Des* 99(1):83–91. <https://doi.org/10.1111/CBDD.13926>
- Zhou W, Ercan D, Jänne PA, Gray NS (2011) Discovery of selective irreversible inhibitors for EGFR-T790M. *Bioorg Med Chem Lett* 21(2):638–643. <https://doi.org/10.1016/j.bmcl.2010.12.036>
- Zubair T, Bandyopadhyay D (2023) Small molecule EGFR inhibitors as anti-cancer agents: discovery, mechanisms of action, and opportunities. *Int J Mol Sci* 24(3):2651. <https://doi.org/10.3390/ijms24032651>

**Publisher's Note** Springer Nature remains neutral with regard to jurisdictional claims in published maps and institutional affiliations.

Springer Nature or its licensor (e.g. a society or other partner) holds exclusive rights to this article under a publishing agreement with the author(s) or other rightsholder(s); author self-archiving of the accepted manuscript version of this article is solely governed by the terms of such publishing agreement and applicable law.

## Authors and Affiliations

Sunil Kumar<sup>1</sup>  · Iqra Ali<sup>2</sup>  · Faheem Abbas<sup>3</sup>  · Nimra Khan<sup>4</sup> · Manoj K. Gupta<sup>5</sup> · Manoj Garg<sup>6</sup> · Saroj Kumar<sup>7</sup> · Deepak Kumar<sup>1</sup> 

✉ Deepak Kumar  
guptadeepak002@gmail.com

<sup>1</sup> Department of Pharmaceutical Chemistry, School of Pharmaceutical Sciences, Shoolini University, Solan, Himachal Pradesh 173229, India

<sup>2</sup> Department of Biosciences, COMSATS University Islamabad, Islamabad Campus, Islamabad 45550, Pakistan

<sup>3</sup> Key Lab of Organic Optoelectronics and Molecular Engineering of Ministry of Education, Department of Chemistry, Tsinghua University, Beijing 100084, People's Republic of China

<sup>4</sup> State Key Laboratory of Biochemical Engineering, Institute of Process Engineering, Chinese Academy of Sciences, Beijing 100190, People's Republic of China

<sup>5</sup> Department of Chemistry, School of Basic Sciences, Central University of Haryana, Mahendergarh, H.R. 123031, India

<sup>6</sup> Amity Institute of Molecular Medicine and Stem Cell Research, Amity University UP, Sector-125, Noida 201313, India

<sup>7</sup> Department of Biophysics, All India Institute of Medical Sciences, New Delhi, India